Characterization of Degraded Drag-Reducing Polymer Solution and its Impact on the Structure of Turbulence

By

Zeeshan Saeed

Bachelor of Science in Mechanical Engineering
Ghulam IShaq Khan Intitute of Engineering Sciences
and Technology,
Topi, Pakistan
2015

Submitted to the Faculty of the
Graduate College of
Oklahoma State University
in partial fulfillment of
the requirements for
the Degree of
MASTER OF SCIENCE
December, 2019

Characterization of Degraded Drag-Reducing Polymer Solution and its Impact on the Structure of Turbulence

Thesis Approved:

Brian Elbing

Thesis Advisor

Omar San

Khaled Sallam

ACKNOWLEDGMENTS

I am grateful to Dr. Elbing for giving me an opportunity to work on polymer drag reduction. I am also grateful to Yasaman Farsiani for mentoring me during this research.

A similar version of the work presented in Chapter II on polymer degradation has been submitted (currently in review) to the Journal of Fluid Engineering (JFE); Farsiani et al. (2019a). This JFE paper was co-authored with Yasaman Farsiani and Dr. Elbing. My contribution to this work was primarily related to the literature review, data acquisition and data analysis. Valuable contributions of Yasaman Farsiani were included in the literature review, data acquisition, data processing and data analysis. Dr. Elbing supervised the research and assisted in every aspect of this study with valuable contributions in the structuring the submission of the research article.

A modified version of the work presented in Chapter III on coherent structures has been submitted (currently in review) to Physics of Fluid (PoF). Farsiani et al. (2019c). The paper was co-authored with Yasaman Farsiani, Dr. Balaji Jayaraman and Dr. Elbing. My primary contributions to this work included the literature review, assisting with experiments and discussion/interpretation of the results. Yasaman Farsiani has primarily involved with data acquisition, data processing and analysis of the results.Dr. Elbing oversaw the entire study, including the experimentation, data reduction and analysis, interpretation of the results and writing the manuscript.

Acknowledgments reflect the views of the author and are not endorsed by committee members or Oklahoma State University.

To my parents, thank you for understanding my absence from home.

To my friends and family, thank you for your support.

And finally to my siblings, I wish they had lived to see this day.

Dedication reflect the views of the author and are not endorsed by committee members or Oklahoma State University.

Name: Zeeshan Saeed

Date of Degree: December, 2019

Title of Study: Characterization of Degraded Drag-Reducing Polymer Solution and its Impact on the Structure of Turbulence

Major Field: MECHANICAL AND AEROSPACE ENGINEERING

Abstract:

Turbulence is often described in terms of either a random process or interacting coherent structures, which is really a choice of which parts of the turbulence to ignore. Focusing on coherent structures reducing the complexity of the problem, which is required to make flow control a possibility. The primary focus of the current study is to analyze how coherent structures within a turbulent boundary layer are modified with the addition of drag-reducing polymer solution (polyethylene oxide, PEO). The performance is known to be concentration dependent, so to mitigate the impact of concentration gradients within the boundary layer the study was performed within a homogeneous polymer ocean. However, this requires the PEO to be exposed to a pump that is known to cause mechanical degradation via chain scission, which significantly impact the polymers behavior. Thus mechanical degradation of dilute PEO solutions was investigated with a turbulent pipe flow setup. Comparative analysis between degraded and non-degraded PEO samples at the same mean molecular weight showed that deviations in the polymer performance scaled with the normalized difference between the initial and final molecular weights. Furthermore, based on literature as well as the current results it was shown that the polymer performance deviations are most likely related to changes in the molecular weight distribution. It was also shown that these deviations could be minimized by increasing the residence time. Limiting the turbulent boundary layer operation conditions to the range where it was shown that the degradation had negligible impact on the PEO performance, allowed a detailed study of the impact of the polymers on the turbulent boundary layer coherent structures. It was observed that the anisotropy of the flow scales increases in proportion to drag reduction, which is consistent with the anisotropy of the fluctuating velocity scales observed in the literature.

TABLE OF CONTENTS

Chapter Page

I Introduction **1**

II Characterization of Polymer Degradation and its Impact on Drag Reduction Performance **5**
- 2.1 Background 5
  - 2.1.1 Polymer drag reduction fundamentals 5
  - 2.1.2 Literature review 9
- 2.2 Experimental Methods 15
  - 2.2.1 Polymer preparation 15
  - 2.2.2 Test facility and instrumentation 17
  - 2.2.3 Data uncertainty analysis 18
- 2.3 Bulk Flow Characterization 20
  - 2.3.1 Non-degraded bulk flow characterization 20
  - 2.3.2 Degraded bulk flow characterization 24
- 2.4 Discussion and Analysis 26
  - 2.4.1 Drag reduction performance 26
  - 2.4.2 Polydispersity 30

III Structure of Turbulence in Polymer Induced Drag Reduction . . **36**
- 3.1 Background 36
  - 3.1.1 Motivation 36
  - 3.1.2 Literature review of Newtonian coherent structures 39
  - 3.1.3 Literature review of drag reduced coherent structures 44
- 3.2 Experimental Overview 46
  - 3.2.1 Test facility and model 46
  - 3.2.2 Instrumentation 47
  - 3.2.3 Polymer preparation and characterization 47
  - 3.2.4 Data analysis 50
- 3.3 Results 51
  - 3.3.1 Mean velocity profiles 51
  - 3.3.2 Newtonian two-point correlations 54
  - 3.3.3 Non-Newtonian two-point correlations 54
- 3.4 Discussion 56
  - 3.4.1 Newtonian two-point correlations and the large scale motions 56
  - 3.4.2 Polymeric two-point correlations and the modified flows . . . 60

IV Summary and Conclusions **64**
4.1 Polymer degradation 64
4.2 Structure of turbulence 67
4.3 Future work 69

REFERENCES **70**

A Polymer Characterization Data **81**

B Intrinsic Drag Reduction Data **83**

LIST OF TABLES

Table Page

2.1 Summary of the range of molecular weights and concentrations tested in the current study as well as the corresponding intrinsic viscosity and overlap concentration for the given molecular weight PEO. 16

2.2 Summary of non-degraded samples tested in the pressure drop apparatus as well as the resulting slope increment (δ), onset wave number (W^*) and the shear rate at the onset of drag reduction (γ^*). 23

2.3 Summary of degraded PEO samples tested in the pressure drop apparatus. 26

3.1 Intrinsic concentrations and drag reduction values for the achieved steady state M_w. Note that %DR here reflects the %DR acheived in tunnel with 100ppm. 49

A.1 P-K plot data points for polymer degradation pertaining to M_{wi} of 5×10^6 (g/mol) to M_{wf} of 1.1×10^6 (g/mol) 81

A.2 P-K plot data points for polymer degradation pertaining to M_{wi} of 5×10^6 (g/mol) to M_{wf} of 2.1×10^6 (g/mol) 81

A.3 P-K plot data points for polymer degradation pertaining to M_{wi} of 5×10^6 (g/mol) to M_{wf} of 3.7×10^6 (g/mol) 81

A.4 P-K plot data points for polymer degradation pertaining to M_{wi} of 4×10^6 (g/mol) to M_{wf} of 1.3×10^6 (g/mol) 82

A.5 P-K plot data points for polymer degradation pertaining to M_{wi} of 4×10^6 (g/mol) to M_{wf} of 1.6×10^6 (g/mol) 82

A.6 P-K plot data points for polymer degradation pertaining to M_{wi} of 2×10^6 (g/mol) to M_{wf} of 0.6×10^6 (g/mol) 82

A.7 P-K plot data points for non degraded polymer pertaining to M_w of 1.0×10^6 (g/mol) 82

B.1 Data corresponding to intrinsic calculations for M_w of 0.7×10^6 g/mol, at concentration of 200ppm for an average %DR of 14.8 83

B.2 Data corresponding to intrinsic calculations for M_w of 0.7×10^6 g/mol, at concentration of 300ppm fo an average %DR of 15.6 83

B.3 Data corresponding to intrinsic calculations for M_w of 0.7×10^6 g/mol, at concentration of 400ppm for an average %DR of 16.7. 84

B.4 Data corresponding to intrinsic calculations for M_w of 1.7×10^6 g/mol, at concentration of 8ppm for an average %DR of 20.6 84

B.5 Data corresponding to intrinsic calculations for M_w of 1.7×10^6 g/mol, at concentration of 20ppm for an average %DR of 30 84

B.6 Data corresponding to intrinsic calculations for M_w of 1.7×10^6 g/mol, at concentration of 30ppm for an average %DR of 36 84

B.7 Data corresponding to intrinsic calculations for M_w of 4.2×10^6 g/mol, at concentration of 25ppm for an average %DR of 33.1 85

B.8 Data corresponding to intrinsic calculations for M_w of 4.2×10^6 g/mol, at concentration of 10ppm for an average %DR of 22.6 85

B.9 Data corresponding to intrinsic calculations for M_w of 4.2×10^6 g/mol, at concentration of 5ppm for an average %DR of 12.6 85

LIST OF FIGURES

Figure Page

2.1 Polymeric velocity profiles from a turbulent boundary layer with non-uniform concentration distribution (Elbing et al. (2013), colored fillers) and channel flow with a constant concentration (Escudier et al. (2009), empty fillers), which shows an increasing slope with increasing drag reduction for HDR ($DR > 40\%$). 14

2.2 Schematic of the pressure drop apparatus used for characterization of the polymer samples as well as mechanically degrading samples. . . . 18

2.3 P-K plot of M_w 2×10^6 g/mol PEO at concentrations of 100, 150 and 500 ppm, as well as water (Newtonian) data at the same range of $\mathrm{Re}\sqrt{f}$. Included for reference are the P-K law, MDR asymptote and logarithmic best-fit curves to the data within the polymeric regime (colored dashed line). 21

2.4 P-K plot using PEO at an initial $M_w = 2 \times 10^6 g/mol$ and c = 500 ppm. One of the samples was degraded to a lower molecular weight ($M_w = 0.6 \times 10^6 g/mol$) while the other was non-degraded 25

2.5 P-K plot comparing degraded and non-degraded samples with $M_{wf} =$ 2×10^6 g/mol or 0.6×10^6 g/mol. Filled markers represent degraded samples, open markers are non degraded at the same mean M_w . . . 28

2.6 Slope increment versus concentration (C) for degraded and non-degraded samples of $M_w = 0.6 \times 10^6$ or 2.0×10^6 g/mol. The dashed lines are all best fit curves with a slope of 0.5 30

2.7 The difference between the degraded and non-degraded slope increments plotted versus the normalized difference between the initial and final molecular weights, $\zeta = (M_{wi} - M_{wf})/(M_{wi})$ 31
2.8 P-K plot comparing a steady-state degraded sample from a C = 100 ppm PEO polymer ocean in a recirculating water tunnel with that of a non-degraded sample. 35

3.1 The mechanistic picture taken from Kline et al. (1967), detailing the proposition of Lighthill (1963) on low speed streak formation. 39
3.2 The Mechanistic picture taken from Kline et al. (1967), displaying vortex liftup and unstable shear layer formation. 41
3.3 The origin of Q_2 and Q_4 events, as displayed in Robinson (1991), during vortex liftup 42
3.4 PIV snapshot of the large scale coherent structures highlighted (at (a) t= 1.0 ms, (b) t= 1.3 ms and (c) t= 1.6 ms 43
3.5 Schematic of the optical arrangement for the PIV measurements, including the nominal location of the field-of-view (FOV). 47
3.6 Inner variable scaled streamwise velocity profiles for water (Newtonian, DR = 0%). The profiles are compared with the viscous sublayer profile ($U^+ = y^+$) and the traditional log-law profile ($U^+ = (ln(y^+)/(\kappa) + B)$ with $\kappa = 0.4$ and B = 5.0. 52
3.7 Inner variable scaled mean streamwise velocity profiles at three drag reduction levels (25%, 58% and 78%) with corresponding Weissenberg numbers listed. The polymer ocean concentration was fixed at 100 ppm and Re_θ=2000. The log-law, ultimate profile and water results (DR = 0%) are also included for comparison 53

3.8 The two-point correlations of the streamwise fluctuating velocities in water (Newtonian) at $Re_\theta = 2000$ for varying reference heights with (b) $\Delta y^+ = 0$ 54

3.9 Two-point correlations of the stream-wise velocity fluctuations with $\Delta y^+ = 0$ and $101 \leq {y_{ref}}^+ \leq 168$ with (a) DR = 0%, (b) DR = 25%, (c) DR = 58% and (d) DR = 78%. 56

3.10 Conceptual picture given by Adrian et al. (2000) on the nested formation of hairpins to form hairpin packets and induce LSMs 59

ABBREVIATIONS

Acronym	**W**hat (it) **S**tands **F**or
CFD	**C**omputational **F**luid **D**ynamics
EIA	**E**nergy **I**nformation **A**dministration
GPC	**G**el **P**ermeation **C**hromotagraphy
kPa	**k**ilo **Pa**scal
LES	**L**arge **E**ddy **S**imulation
MDR	**M**aximum **D**rag **R**eduction
N-S	**N**avier-**S**tokes
PAM	**P**oly **A**crylamide
PDEs	**P**artial **D**ifferential **E**quation
PDR	**P**olymer **D**rag **R**eduction
PEO	**P**oly **E**thylene **O**xide
P-K	**P**randtl-**K**arman
ppm	**p**art **p**er **m**illion
RANS	**R**eynolds-**A**veraged **N**avier-**S**tokes equation
TBL	**T**urbulent **B**oundary **L**ayer
THF	**T**etra **H**ydro **F**uran
TKE	**T**urbulent **K**inetic **E**nergy
US	**U**nited **S**tates

CHAPTER I

Introduction

With increasing concerns on the available energy resources, the push for improved and more efficient systems has been more than ever before. According to a recent survey conducted by the US. Energy Information Administration (EIA), the greatest share of energy consumption belongs to the transportation sector, which consumes about 37% of the total available energy (U.S. EIA, Monthly Energy Review, April 2019). Next on this list is the industrial sector which consumes about 35% of the energy produced in the US. This topped by the fact that US is also the leading energy consumer per capita in the world, makes such energy/power related topics so concerning that a tremendous amount of effort has been employed to solve these energy issues. Lately, public awareness campaigns have been initiated towards the use of renewable energy resources, but the usage and development of such resources is hindered by many socio-political factors. Changing public aptitudes, especially considering the ease of usage offered by the non-renewable resources (e.g. fossil fuels) and the economies associated with the non-renewable resources make such renewable energy technological changes to be in their nascent stages. This is also reflected in the most recent statistical survey conducted by the EIA (U.S. EIA, Monthly Energy Review, April 2019), which shows that less than 12% of the total energy produced comes from renewable energy sources such as the wind, solar and geothermal energy. On the parallel, there has been a growing concerns about the impact of emissions resulting from the burning of fossil fuels (oil, gas and coal) on the global climate. Institutional meetings, such as the Paris Climate Agreement, are now being summoned more frequently than before

to urge nations with significant carbon footprints to take necessary steps in hopes to mitigate such effects by decreasing emissions and finding ways of making the already existing systems more efficient. In other words, ways are to be developed so that the per unit cost of energy produced, there is a reduction in the amount of fossilized fuels burnt (i.e. burnt in a more efficient way).

In the context of scenario presented above, methods for reducing drag in fluid flow applications find immense potential for their utilization. One such method has been focused in the current study; polymer drag reduction (PDR). PDR is an active flow control technique that has already demonstrated great practical utility in oil transportation through pipelines, sewage systems and fire hoses to mention a few (Sellin et al. 1980). While various avenues of its potential usage are still being explored, many attempts are concurrently being made on fundamental grounds to understand various aspect of this flow control technique. The current study is an example of one such attempt. This study primarily focuses on the behavior of polymers in fluid flow applications and tries to connect the observations recorded with literature and seeks an explanation, being consistent with the literature, for the observed effects.

As has been mentioned above, PDR has a whole lot of potential for the transportation and industrial sectors, but the effectiveness of this method is significantly dependent on and limited by one very crucial parameter, which is intrinsic to the polymer itself. This factor is that of the polymer degradation under immense flow strains, of which turbulent flows are a rich source of. Such strain induced polymer breakdown is referred to as "mechanical degradation of polymer molecule chains." This results in the shortening of the polymer chains, by virtue of their breakdown under stressed states, because of the superimposed strains of the flow field. This is a critical issue because the efficiency of the polymer is dependent on the polymer molecule chain length, with the effectiveness of the polymer as a drag reducing agent being proportional to its chain length. Studies, such as Habibpour and Clark

(2017), show that historically such degradation issues have conveniently been avoided by either assuming such degradations effects to be negligible or by using grades of polymer that are resistant to such chain cleavages thereby, making such degradations to be of secondary importance. However, using such degradation-resistant polymers compromises their drag reducing efficiency and therefore makes their practical application less promising, especially for transportation (external) applications. Also, the rheological aspects of the problem suggest that such a degradation is a natural cause-and-effect type event if drag reduction is to be affected. Therefore, characterization of the polymer degradation has to be done for a complete and meaningful analysis. This serves the motivation behind the first half of the current study. A pre-print of this study can be found as Farsiani et al. (2019b).

The second half of the study focuses on providing a potential explanation for the observed effect of drag reduction using polymer additives in light of literature and results obtained in experiments recently conducted for Farsiani et al. (2019c). This section focuses on providing an explanation in terms of modified structure of turbulent flow when polymer additives are used. Several physical mechanisms for the basic turbulent flow structure have been proposed since the mid 1950's. Due to lack of computational capacities, such hypothetical models have mostly relied on sheer intuition of the subject coupled with the limited experimental observations of the time. It was not until the numerical capacities of computers which begun to improve, and it continues to be the case even today, that some of such hypothetical models were tested and found to be mathematically relevant, as well as being physically sound, to help explain the much elusive and sought after structure of turbulence in the near wall region. The fact that Reynolds Averaged Navier-Stokes (RANS) equation bears the Reynolds shear stress term, points to the idea that turbulence has both a mechanism and associated structures facilitating such mechanism, particularly in the near wall region. Such phenomenology is cardinal to the structure of turbulence

research. Though much work has been done in this regard, a latest insight have shown that such developments are incremental of a complex system. Such a discussion forms the second half of this study. Selected models, which have favorably gathered the support of experimental evidence on near wall turbulent boundary layer structure, have been analyzed in light of the most relevant literature available as well as the data gathered in Farsiani et al. (2019c).

The remainder of this thesis is divided into two main sections. The first section shows the study done with regard to polymer degradation. Polymer degradation section comprises of the literature review as well as a detailed explanation on the experimental setup employed coupled with the uncertainty analysis of the data. Then, the results from this study are presented and discussed to reach the conclusions derived at the end of this section. The second section provides a detailed introduction to the structure of turbulence; the theory of coherent structure for near wall turbulent flows. Potential effect of polymers on such structures is then provided in attempt to offer a possible explanation on mechanism for PDR.

CHAPTER II

Characterization of Polymer Degradation and its Impact on Drag Reduction Performance

2.1 Background

2.1.1 Polymer drag reduction fundamentals

A brief review of the PDR fundamentals is given for the sake of completeness as well as to provide the relevant knowledge to the readers for the forthcoming analysis. Experiments conducted to evaluate the impact of mechanical degradation on the drag reducing performance of the polymer have been done in pipe flows. For this reason, principles of turbulent pipe flows have also been discussed. The findings in the current study are presented in terms of the traditional Prandtl-von Karman (PK) plots; $f^{-1/2}$ plotted on the ordinate axis and $Re_d f^{-1/2}$ plotted on the abscissa axis. Here f refers to the Fanning friction factor, whereas Re_d is the nominal pipe diameter-based Reynolds number. Although the Fanning friction factor could be directly retrieved by measuring the wall shear stress as shown in its defining Eq. (2.1), such a measurement is especially difficult to make in pipe flows. For this reason, in the current study, the Fanning friction factor was estimated using pressure-differential measurements, Δp through the relation given in Eq. (2.2).

$$f = \frac{2\tau}{\rho {U_{avg}}^2} \tag{2.1}$$

$$f = \frac{D}{2\rho {U_{avg}}^2} \frac{\Delta p}{\Delta x} \tag{2.2}$$

Here Δx is the section length of the pipe between which the pressure-differential measurements were taken. There is an implicit assumption that is automatically made while using Eq. (2.2) and it is that of a fully developed pipe flow. This assumption has been taken into consideration in experimental as well as while analyzing the results. In the canonical sense, much of the literature has presented the data in terms of the P-K plots. This has been one of the reasons for choosing these coordinates for data presentation. Besides such canonical reasons for its selection, P-K plots also naturally depict an accurate estimate of the various flow scales in comparison with the pipe scales; the ordinate is the ratio of the bulk fluid velocity to the turbulent friction velocity whereas the abscissa represents the ratio of pipe scales to turbulent length scales. The convenience of using P-K plots can also be realized by seeing that it incorporates the friction-law for fully turbulent smooth pipe flows. Mathematically, this friction law is expressed as given in Eq. (2.3),

$$\frac{1}{f^{(1/2)}} = 4.0 log_{10}(Re_d \frac{1}{f^{(1/2)}}) - 0.4. \tag{2.3}$$

The polymeric flow results have also been computed and have been shown to have excellent agreement with the friction-law for the non-polymeric (Newtonian) case. Another important feature represented by P-K plots is that of the maximum drag reduction asymptote (MDR), which was empirically determined by Virk et al. (1967) in the form

$$\frac{1}{f^{(1/2)}} = 19.0 log_{10}(Re_d \frac{1}{f^{(1/2)}}) - 32.4. \tag{2.4}$$

The accuracy of this asymptotic relation has been verified in a number of studies. This has been experimentally and numerically verified by Virk et al. (1970) and Ptasinski et al. (2001), respectively. The MDR asymptote represents the highest possible value for drag reduction that can be achieved and so is a limiting case, as is the Newtonian flow (representing 0% drag reduction) for smooth pipes. In this way P-

K plots clearly conveys the behavior of three different regimes; Newtonian, MDR and the intermediary regime of polymeric flows between the two aforementioned regimes. This investigation primarily investigates the specifics in the polymeric regime.

Given this scheme of data presentation, we now turn to the real subject matter; impact of mechanical degradation of polymers on PDR. Polymers have been known to reduce friction in pipe flows since Toms (1948) first made such observations. The subject of PDR is at the intersection of two very complex, but interesting, fields; turbulence and rheology. A number of studies attest to the fact that the intrinsic properties of polymer chains are crucial in controlling the flow properties and strongly influence/control the overall bulk-flow behavior observed, both in the literature as well as in the current study. Of particular significance is the property of such polymer chains to stretch when in strain fields and the ensuing effects of such a stretch on the polymer properties. Such intense strain fields are one of the mainstream features of turbulence, particularly in the near wall region. Therefore, this tendency of polymer chains to get stretched under the influence of the flow results in the chain being stressed, causing them to break when these stresses cross a certain threshold. As has been mentioned in the introduction, this cleavage of polymer chains has been termed mechanical degradation. The break down of the polymer chains is itself indicative of the idea that the polymer molecules actively interfere with the flow dynamics and therefore, are engaged in rerouting the energetics of the flow to effect drag reduction. However, there is one important concept that has been found to be central in this drag reduction observation. In a flow field, polymer molecules will generally be stretched, but as they are being randomly convected in the wall-normal region the polymer molecules experience flow regions with varying time scales. Given this range of time scale, there is another time scale associated with the polymer molecules and is dependent on the intrinsic properties of the polymer such as it chain lengths and M_w (molecular weight). This time scale characterizes the amount of

time the polymer molecule takes to attain its equilibrium conformation (the no stress state), after being stretched by the flow field (i.e. the time scale associated with the relaxation of polymer molecule). Such a time scale is quantified by a dimensionless number which is crucial to the study of PDR, Weissenberg number. Weissenberg number (We) is the ratio of the polymer relaxation times to the local flow time scales. In general, the higher the We, the greater the drag reduction. Note that the drag reduction is observed even if the We is less than 1. Since the time scales cannot be negative, We is always greater than zero. As is apparent from the definition, We represents the ratio of the intrinsic polymer properties to the flow properties and so, bridges the rheological aspect of the problem with the flow mechanics.

Another important concept associated with polymer sciences is that of polymer sample being mono-disperse or polydisperse. As will be seen in the Results and Analysis section, polydispersity relays an important information regarding the flow properties of polymer solutions. Here only a brief introduction on these sections is given. A mono-disperse sample is a sample that contains only a single type of polymer molecule chain for which the molecular weight of a sample is an accurate measure. It is to say that in a given monodisperse sample of polymer, each molecule chain is essentially identical to all other chains present in that sample. However, for a polydisperse sample the scenario is quite different. In contrast to a monodisperse sample, a polydisperse sample has a range of polymer molecule chain lengths (i.e. polymers with varying M_w). The molecular weight of such a sample is reported to be as average molecular weight as opposed to just a single molecular weight reported for a mono-disperse samples. The reported average molecular weight for a polydisperse sample represents the dominant chain fraction of the polymer molecule present in a given sample. It is worth mentioning that practically most of the samples commercially produced are poly-dispersed as opposed to mono-dispersed. In the same vein, the samples used in this study are polydisperse.

2.1.2 Literature review

The ability to reduce skin-friction with polymer solutions, historically referred to as Toms effect, has been known since the late 1940s. Some of the first investigations on this include that of Mysels (1949), Toms (1948) and Toms (1949). Since that point, there have been numerous successful studies that have produced various applications. A comprehensive review on this is given by Hoyt (1972) while more focused applications on internal flows can be found in Burger et al. (1980) and Sellin et al. (1982). Most active research in polymer drag reduction (PDR) focuses on developing a fundamental understanding of PDR to enable external flow applications such as marine vehicles. This has been the motivation behind many studies including that of Fruman and Aflalo (1989), White and Mungal (2008), Elbing et al. (2010a), Elbing et al. (2010b), Elbing et al. (2011), Elbing et al. (2013) and Perlin et al. (2016). One of the primary limiting factors for advancing PDR to external flows (as well as expanding internal flow applications) is polymer degradation. Polymer degradation is known to be dependent on many initiating factors such as oxidative and bacterial action, free radical interaction (chemical degradation), thermal degradation and mechanical degradation. A detailed account on such varying range of polymer degrading factors can be found in McGary Jr (1960), Shin (1965) Jr FE and Koleske (1976), Bortel and Lamot (1977), Moussa and Tiu (1994) and Fore et al. (2005), to name a few. The aging of polymer solution has also been found to contribute to polymer solution degradation, as shown in Layec-Raphalen and Layec (1985). The current study, however, focuses solely on degradation due to chain scission induced from turbulent flow structure-polymer chain interaction (i.e., mechanical degradation in a turbulent pipe flow). Many accounts on theoretical/computational models detailing the mechanics of the physical process of polymer-chain degradation based on their interaction with the basic turbulent flow structures (e.g. horseshoe/hairpin vortices). For a more detailed and mathematically comprehensive approach, the reader is referred to work of

Yarin (1991).

While the literature for polymer degradation (mostly for internal flows) is vast, a brief review of key papers that influence the current work is provided here for completeness. The flow induced shear (mechanical force) on the polymer chain can be generated from abrupt changes in flow geometry (e.g. pumps, valves and perforations) as shown in Zaitoun et al. (2012). Large mean velocity gradients, such as those experienced at the wall of high Reynolds number turbulent flows, also result in flow induced shear (mechanical force) as discussed in Elbing et al. (2011); Fontaine et al. (1992), Petrie et al. (2005) and Elbing et al. (2009). Initial studies, such as that of Culter et al. (1975), discovered that it was extremely challenging to produce a setup that could isolate the degradation to the flow region of interest. Moussa and Tiu (1994), Elbing et al. (2009) and Vanapalli et al. (2005), as a series of more recent studies, have concluded that the majority of the degradation was produced at the entrance to their test facility.

Paterson and Abernathy (1970) was one of the earliest investigations on the impact of flow-assisted (mechanical) degradation on the molecular weight distribution (e.g. polydispersity), which it concluded that degradation influences the resulting flow properties. Yu et al. (1979) used monodisperse polystyrene and polydisperse polyisobutene samples in oils under high shear rates to show that the molecular weight distribution narrowed for the poly-dispersed samples and only had a slight broadening of the monodispersed sample. More specifically, the distributions revealed that the breaking of the chains was not a random process. Hinch (1977) developed a formula estimating the required force to break a molecular chain at a given location within the chain. This theoretical evaluation showed that the maximum strain developed in stretching the chain was at its center. Subsequently, Horn and Merrill (1984) showed that turbulence induced scission of macromolecules in dilute solutions preferentially break at the midpoint of the chain. Moreover, Odell et al. (1983) studied extensional

flows produced in cross slot devices with low molecular weight ($M_w < 10^6$) polyethylene oxide (PEO), which was at sufficiently low molecular weights for measurements of the molecular weight distribution. These results showed that the molecular weight distribution had another peak in addition to the original one at half the molecular weight, indicating scission of the chain at its midpoint. More recently, a simulation of flow-induced polymer chain scission by Sim et al. (2007) validated the midpoint scission hypothesis under the condition that the elongation rate was comparable to the critical elongation rate, then the instantaneous segmental tensions attains a maximum at the chain midpoint. This has the consequence of the resulting daughter chains having a rather narrow distribution. However, it was also demonstrated that when the elongational rate is much larger than the critical elongational rate, scission can occur in the partially coiled chains resulting in scission occurring farther from the midpoint. This likely has a significant impact within wall-bounded turbulent flows where the stress distribution varies significantly from the maximum at the wall to very weak away from the wall (e.g. pipe centerline or outside of a turbulent boundary layer).

Hunston and Zakin (1980) used turbulent drag reduction (similar to current study), viscosity and gel permeation chromatography (GPC) on polystyrene samples to assess the influence of concentration, molecular weight and molecular weight distribution on flow-assisted (mechanical) degradation. This showed that the onset of drag reduction provided information about the largest molecules in the flow while the flow rate dependence was related to the shape of the top part of the molecular weight distribution. Gampert and Wagner (1985) used laboratory synthesized straight molecular chain polyacrylamide (PAM) in aqueous solutions to investigate the influence of molecular weight and polydispersity on drag-reducing effectiveness. Gampert and Wagner (1985) artificially created polydispersity by mixing the high and low synthesized molecular weights in a single solution. This work made several con-

clusions that are consistent with available literature. Primarily, that the long chain molecules are pivotal in determining the flow properties of a solution due to their preferential mode of extension and hence degradation, when the difference in size of existing chains in a solution is reasonably high within a suitable range of Reynolds number.

Historically, mechanical degradation has significantly limited the viable applications for PDR since polymers are generally more efficient at reducing drag (i.e. require lower concentrations to achieve a desired drag reduction) the longer the polymer chain (i.e. higher molecular weight), but the longer the polymer chain the more susceptible it is to chain scission. Internal flows have typically avoided this problem by using stiffer polymers (e.g. PAM), and some applications, as given in Gampert and Wagner (1985), have shown an increase in resistance to mechanical degradation with increasing concentration. But the use of commercial grade PAM is not suitable for investigations involving the influence of molecular weight on drag reduction and mechanical degradation because they have a branched chain formation and the presence of copolymers, as discussed by Gampert and Wagner (1985). Instead, PDR studies have focused primarily on high molecular weight PEO, as has been the case in external flow studies, because PEO has the ability to achieve (MDR) with concentrations on the order of 10 parts-per-million (ppm). In addition, PEO avoids the rheological issues faced with commercial grade PAM. The high efficiency of PEO is ideal for external flows, which continuously dilute the injected polymer solution into the developing boundary layer. However, as a result, polymer degradation has had a significant impact on PDR external applications and even the ability to study PDR within turbulent boundary layers.

Elbing et al. (2011) developed a fundamental scaling law for the evolution of the mean molecular weight within a developing high-shear turbulent boundary layer, which requires an estimate of the steady-state molecular weight for the given lo-

cal shear rate. This was produced from the universal scaling law for chain scission given by Vanapalli et al. (2006). This scaling works provided that the nominal bond strengths for carbon-carbon and carbon-oxygen bonds are 4.1 nN and 4.3 nN, respectively, as detailed by Grandbois et al. (1999). In light of this observation, a review of literature that has reported PDR modifications to the near-wall velocity profile of a turbulent boundary layer with PEO is worth a mention. Such work includes Elbing et al. (2013), Fontaine et al. (1992), Petrie et al. (2005), White et al. (2004), Hou et al. (2008) and Somandepalli et al. (2010), and shows that many of the conditions reported by Elbing et al. (2013), Fontaine et al. (1992) and Petrie et al. (2005), experienced significant changes in the mean molecular weight between the injection and measurement locations even though this was not accounted for in their analysis. This is particularly problematic when studying high drag reduction (HDR; $> 40\%$ DR), which recent computational work of White et al. (2012) and experimental efforts of Elbing et al. (2013) and Escudier et al. (2009) (see Figure 2.1; where the streamwise velocity and wall-normal distance are scaled with inner variables) have shown that modifications to the near-wall velocity profile deviate from the classical view that assumes the near-wall momentum distribution is independent of polymer properties. Elbing et al. (2013) showed that Reynolds number was insufficient to collapse the available experimental turbulent boundary layer data, which suggests that the remaining scatter in the results must be related to polymer properties. These polymer properties are sensitive to the molecular weight, which means that in addition to an evolving polymer concentration distribution, there is also an evolving molecular weight distribution that needs to be accounted for to properly study HDR in a turbulent boundary layer. Recently this has motivated an alternative approach adopted in Farsiani et al. (2019c), which is to develop a polymer ocean at a uniform concentration that has been mechanically degraded to a steady-state molecular weight. Then the developing boundary layer would have a known and uniform polymer concentration

and mean molecular weight. However, this requires a proper understanding of the impact of mechanical degradation via chain scission on the drag reduction performance of PEO, which is the focus of the current study. Specifically, the current study prepares degraded and non-degraded samples at the same mean molecular weight and does a comparative analysis of their drag reduction performance.

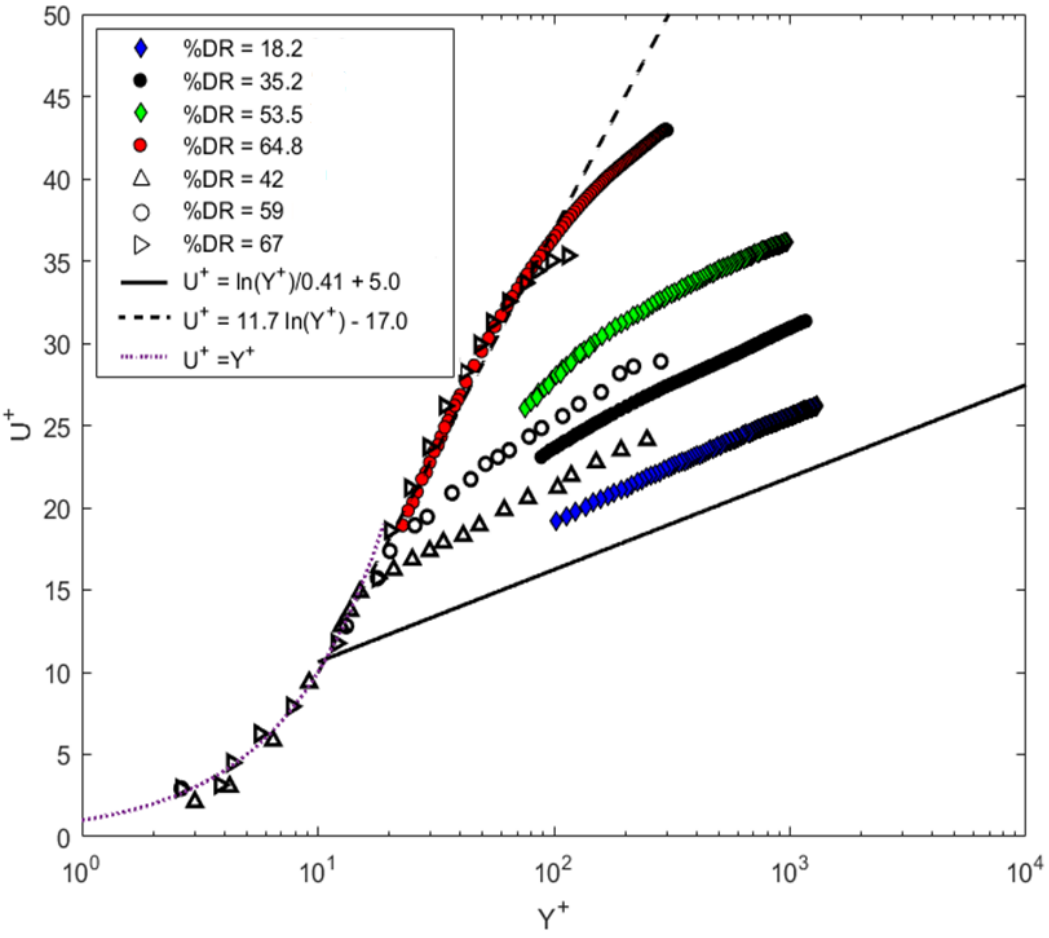

Figure 2.1: Polymeric velocity profiles from a turbulent boundary layer with non-uniform concentration distribution (Elbing et al. (2013), colored fillers) and channel flow with a constant concentration (Escudier et al. (2009), empty fillers), which shows an increasing slope with increasing drag reduction for HDR ($DR > 40\%$).

2.2 Experimental Methods

2.2.1 Polymer preparation

PEO was the only polymer used in this study, which has a structural unit (monomer) of $\text{——O—CH}_2\text{—CH}_2\text{——}$ that results in a polymer backbone consisting of carbon-carbon C——C and carbon-oxygen C——O bonds. Five molecular weights of PEO were tested with manufacturer specified mean molecular weights of 0.6, 1.0, 2.0 and 5.0 $\times 10^6$ g/mol (Sigma Aldrich, model #: 182028-250G, 372781-250G, 372803-250G, 189472-250G,) and 4.0×10^6 g/mol WSR301 (Dow Chemicals). As previously stated, these high molecular weight polymers are highly susceptible to mechanical degradation within shear flows. Degradation depends on the molecular weight, polymer concentration, solvent type, turbulent intensity and flow geometry as shown in Kim et al. (2000) and Kalashnikov (2002). Polymer solutions were prepared by sprinkling dry powder into a water jet prior to contacting the free surface to avoid formation of polymer aggregates. Draad et al. (1998) and Petrie et al. (2003) have shown that chlorine in the solvent (water) can cause polymer degradation. Therefore, when solutions required hydration longer than 12 hours the background chlorine was removed by adding trace amount of sodium thiosulfate, which residual sodium thiosulfate and the resultant products of the reaction with chlorine has been shown to not impact the PDR performance, as shown in Petrie et al. (2003). Stock solutions were prepared at relatively high concentrations ($1000-5000$ ppm), which once fully hydrated, additional water was added to dilute the sample to the desired test concentration.

Polymer solution concentrations are broadly categorized as dilute, semi-dilute and concentrated. In the dilute regime, each polymer chain is sufficiently distant from other polymer chains such that there is minimal interaction between chains. As the concentration increases, polymer chains eventually begin to overlap and become entangled, which these interactions alter the polymer properties. As the concentration

further increases from semi-dilute to the concentrated regime, molecules cannot move freely and significant interpenetration occurs due to the lack of space. These changes are identified from their rheological properties as shown in De Gennes and Gennes (1979). The critical overlap concentrations C^* and C^{**} define the transition points from dilute to semi-dilute and semi-dilute to concentrated regimes, respectively. The first overlap concentration can be found from the inverse of the intrinsic viscosity η_0 , $C^*=\frac{1}{\eta_0}$, which η_0 can be estimated from the Hark-Houwink relationship given in Bailey Jr. and Callard (1959), $\eta_0 = 0.0125\ M_w^{0.78}$. Table 2.1 provides the range of molecular weights and concentrations tested for degraded and non-degraded samples in this study as well as the corresponding intrinsic viscosity and C^*. The first overlap concentration was well above the test range at each molecular weight and, consequently, all testing was with dilute solutions.

Table 2.1: Summary of the range of molecular weights and concentrations tested in the current study as well as the corresponding intrinsic viscosity and overlap concentration for the given molecular weight PEO.

$M_w \times 10^{-6}$ (g/mol)	C range (ppm)	$[\eta]_0$ cm^3/g	C^* (ppm)
0.6	100-500	402	2500
1	500	598	1680
2	50-500	1030	975
4	5-100	1760	568
5	5-20	2100	477

2.2.2 Test facility and instrumentation

The primary test facility was a pressure drop apparatus that was used to characterize polymer properties and acquire the gross flow behavior. A schematic of the setup is shown in Figure 2.2, including the pipe as well as the instrumentation. Test samples were placed in an 18.9-liter 316L stainless steel pressure vessel (740560, Advantc), which was sealed and pressurized to 275 kPa during testing. A dip tube drew the polymer sample from the bottom of the pressure vessel and then pushed it into the pipe flow portion. It consisted of a 10.9 mm inner diameter (d) instrument grade seamless 316 stainless steel pipe (SS-T8-S-035-20, Swagelok) that was divided into 3 sections; the entrance length that was $150d$ long to achieve fully developed turbulent pipe flow, a 1.05 m long test section and the end (exit) length that had a V-shaped, 4.8 mm orifice needle valve at the outlet to control flowrate (this valve was also used as the primary means to accelerate the degradation of the polymer solutions). Given the valve properties and the current operation range, the maximum flow coefficient was nominally 0.22. The pressure drop across the test section was acquired at various Reynolds numbers with a differential pressure transducer (PX2300-5DI, Omega Engineering). The mass flowrate, and ultimately the average velocity within the pipe, was determined by measuring the mass of a sample on a 35 kg digital balance (CPWplus-35, Adam Equipment) while simultaneously recording the fill time with a stopwatch (RS-013, ProCoach). A more detailed discussion of the setup, instrumentation and uncertainty quantification is provided in Lander (2018).

Polymer solution temperature was measured with a thermometer (25-125°F, TEL-TRU) and was held relatively constant throughout testing at 21 ± 0.4 °C with a corresponding mean density (ρ) and kinematic viscosity (ν) of 998 kg/m^3 and 1.0×10^{-6} m^2/s, respectively. The pipe diameter and pressure drop length had uncertainties below 1%. Given the high accuracy of the pressure transducer ($\pm$0.25%), the largest uncertainty in the differential pressure was due to the experimental setup. Specifi-

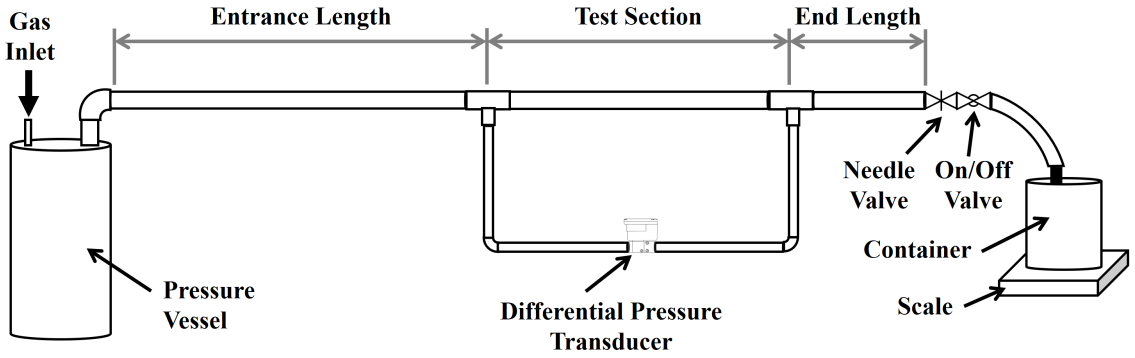

Figure 2.2: Schematic of the pressure drop apparatus used for characterization of the polymer samples as well as mechanically degrading samples.

cally, the holes in the pipe walls (pressure taps) required for the measurements were the largest source of error. Corrections were applied following the approach outlined in the chapter McKeon from Tropea and Yarin (2007) with the corresponding uncertainty of 3% for the pressure measurement. The mass flowrate was determined from measuring the fill time and mass during data collection. There are several sources of errors that were considered. The details on the nature of such errors is given in Lander (2018). The largest source of error in this investigation, however, was the limitation of human reaction times. This resulted in uncertainties as large as 3%, but by increasing the measurement period (especially for low flow rate conditions) this uncertainty was reduced.

2.2.3 Data uncertainty analysis

Propagating all sources of uncertainty results in uncertainties that significantly vary with flow condition resulting in Prandtl-von Karman (P-K) coordinates $Ref^{1/2}$ and $1/f^{1/2}$ having typical uncertainties of 6%. However, at low flow rates (i.e. at and below the onset of drag reduction) the uncertainty increases rapidly to well above 10% as shown in Lander (2018). For these reasons measurements at the onset of drag reduction were not attempted, but rather measurements at higher flow rates with uncertainty below 10% were curve fitted and then extrapolated back to the onset

condition. Subsequently, the analysis focuses on the variations of the slopes of these curve fits, so a more detailed uncertainty analysis on the impact of these uncertainties in the P-K coordinates on the slope and intercept of the curve fits was performed. Here, error was introduced to each of the P-K coordinates such that a logarithmic curve fit takes the form given in Eq. (2.5),

$$\frac{1}{\sqrt{f+\epsilon_0}} = C_0 \ln(Re\sqrt{f} + \epsilon_1) + C_1, \tag{2.5}$$

where C_0, C_1 are constants and ϵ_0, ϵ_1 are the uncertainties in f and $Re\sqrt{f}$, respectively. Some algebraic manipulation and expanding the resulting expression in a binomial form results in (2.6),

$$\frac{1}{\sqrt{f}}(1 - \frac{\epsilon_0}{2f} + \cdots) = C_0 \ln(Re\sqrt{f}) + C_0 \ln(1 + \frac{\epsilon_1}{Re\sqrt{f}}) + C_1. \tag{2.6}$$

Neglecting higher order terms and some addition and then rearranging reduces the relationship to (2.7),

$$\frac{1}{\sqrt{f}} = C_0 \ln(Re\sqrt{f}) + C_0 \ln(1 + \frac{\epsilon_1}{Re\sqrt{f}}) + C_1 + \frac{\epsilon_0}{2f^{3/2}}. \tag{2.7}$$

Treating the error sources as being nominally constants, this shows that the uncertainty impacts the intercept more than the slope when $Re\sqrt{f}$ is large (current data $Re\sqrt{f} > 10^3$).

Like many previous degradation studies, such as Moussa and Tiu (1994), Elbing et al. (2009), Hunston and Zakin (1980), Kim et al. (2000) and Kulik (2001), the current work utilizes the drag reduction performance (determined from its behavior in this pressure drop apparatus) to investigate degradation. GPC and other such methods are preferred since they provide direct measurements of the molecular weight distribution, but GPC has proven to be impractical for high molecular weight PEO

due to significant uncertainties in the analysis. One of the main issues that complicates this approach is that while PEO is soluble in tetrahydrofuran (THF), a common eluent for GPC, it is isorefractive with THF. This makes it so that it cannot be seen in that solvent with either index of refraction or light scattering detectors as mentioned in Elbing et al. (2018). Another significant limitation in the use of GPC for estimating the polydispersity comes from its incapability to resolve low molecular weight fractions for PEO molecular weights as low as 2.5×10^5 g/mol. This has been explicitly stated in Berman (1977). Such lower molecular weight fractions are known to significantly affect the number average molecular weight of a sample necessary to evaluate polydispersity as described in Gampert and Wagner (1985) and Berman (1977). This renders the use of GPC for high molecular weight samples ineffective and so has not been made use of in this investigation. Thus, the current study quantifies the impact of mechanical degradation via chain scission on the drag reduction performance of PEO primarily from the resulting variations in the turbulent drag reduction performance. Based on previous studies using other polymer solutions, the likely impact on the molecular weight distribution is inferred.

2.3 Bulk Flow Characterization

2.3.1 Non-degraded bulk flow characterization

It is common to present pipe flow skin-friction results in either a Moody diagram (Darcy-Weisbach friction factor versus Reynolds number) or in P-K coordinates ($f^{-1/2}$ versus $Re_d f^{1/2}$). For the current study, P-K coordinates are used, where ($Re_d = (\rho V d)/(\mu)$) is pipe diameter-based Reynolds number, f is the Fanning friction factor ($f = (2\tau)/(\rho V^2)$, ρ is the fluid density, V is the mean velocity, d is the pipe diameter, μ is the fluid dynamic viscosity and τ is the wall shear stress. Assuming fully developed pipe flow, the wall shear stress (τ) is directly related to the pressure drop across a given length of pipe, Eq. 2.2. The physical significance of P-K plots is that the ordinate

is the ratio of the bulk fluid velocity to the turbulent friction velocity (divided by $\sqrt{2}$) and the abscissa is the ratio of the pipe diameter (outer length scale) to the viscous wall unit (inner length scale) (multiplied by $\sqrt{2}$). The skin-friction curve for Newtonian turbulent pipe flow in these coordinates is well represented by the P-K law, Eq. (2.3). Newtonian (water) results from the current setup are included in Figure 2.3. These results are well approximated by the P-K law, Eq. (2.3), which is also included for comparison.

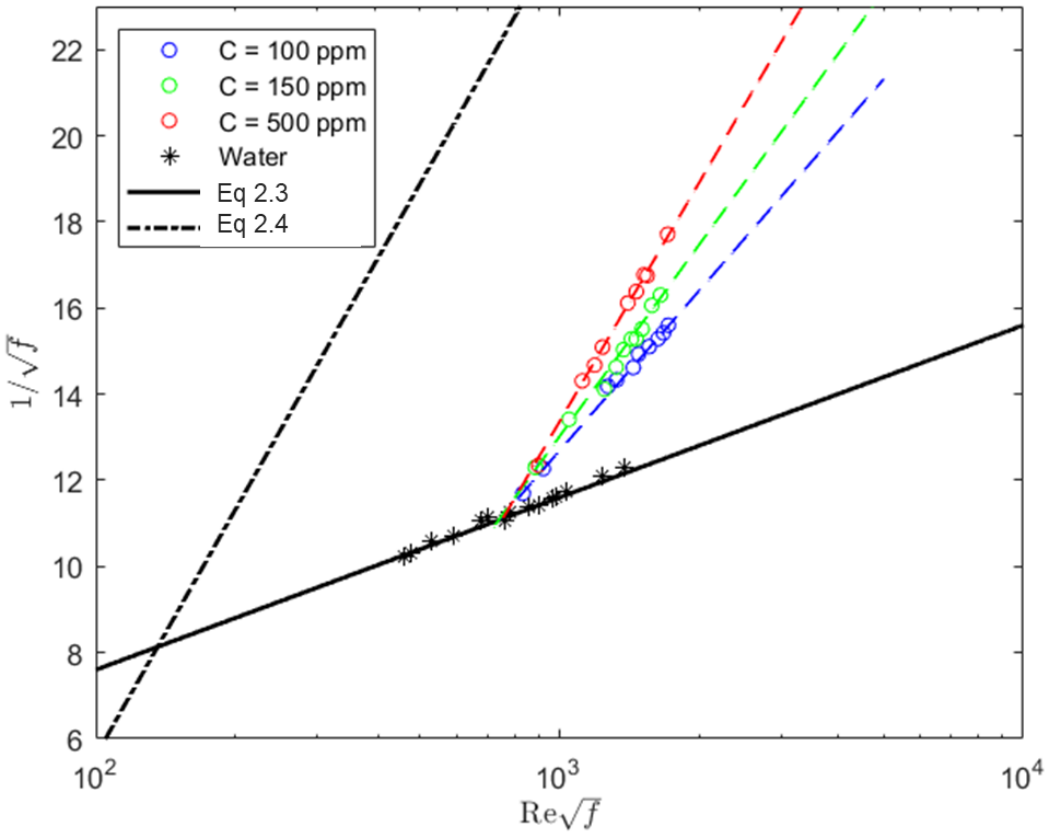

Figure 2.3: P-K plot of M_w 2×10^6 g/mol PEO at concentrations of 100, 150 and 500 ppm, as well as water (Newtonian) data at the same range of $\mathrm{Re}\sqrt{f}$. Included for reference are the P-K law, MDR asymptote and logarithmic best-fit curves to the data within the polymeric regime (colored dashed line).

With the addition of drag reducing polymer (PEO) solution, the results are shifted above the P-K law. The amount of increase is limited by the empirically derived MDR asymptote, as shown in Virk et al. (1967). This is given in Eq. (2.4). The current

study focuses on results within the polymeric region, which is at intermediate drag reduction levels between the MDR asymptote and the P-K law. The data within the polymeric regime are fitted following the form given in Eq. (2.8) from Virk (1975),

$$\frac{1}{f^{(1/2)}} = (4.0 + \delta) log_{10}(Re_d \frac{1}{f^{(1/2)}}) - 0.4 - \delta log_{10}(2dW^*). \tag{2.8}$$

Here δ is the slope increment and W^* is the onset wave number, which both are dependent on the polymer properties. Furthermore, the slope increment δ is the change in slope relative to the P-K law slope, and the onset wave number W^* can be shown to be equal to the reciprocal of the viscous wall unit at the onset of drag reduction. The onset of drag reduction is identified by the intersection of the P-K law and the polymeric data fitted with Eq. (2.8). Note that below this minimum shear rate required to initiate drag reduction, the polymer solutions follow the P-K law, which is indicative of the need for a sufficient amount of shear to stretch the polymer chains and active the drag reduction mechanism, as discussed in Dubief et al. (2004) and Gupta et al. (2004). The onset of drag reduction for a given polymer type and molecular weight has been shown to have a negligible dependence on the concentration here. This is consistent with the findings of Vanapalli et al. (2005) and Virk (1975). Current polymeric results using PEO at a $M_w = 2 \times 10^6$ g/mol and at concentrations from 100 to 500 ppm are also provided in Figure 2.3. These results show that the slope increment increases with increasing polymer concentration (C) while the onset of drag reduction (intersection of P-K law and polymeric data fit) remains nearly constant for all three samples tested.

While the onset of drag reduction remains constant for a given molecular weight, it is sensitive to the mean molecular weight. Generally, the higher the M_w the lower the Reynolds number at the onset of drag reduction. Vanapalli et al. (2005) compiled PEO data from Virk (1975) to establish an empirical relationship between the onset of drag reduction shear rate γ^* and the mean molecular weight M_w, $\gamma^* = (3.35 \times 10^9 / M_w)$.

This allows for the mean molecular weight to be determined if the wall shear rate at the onset of drag reduction is known. The wall shear rate at the onset of drag reduction is determined by calculating the intersection between the polymeric best-fit curve and the P-K law. The intersection provides the corresponding onset of drag reduction Fanning friction factor (f^*) and the onset of drag reduction Reynolds number ($Re_d{}^*$). Given the definition of the Fanning friction factor and the relationship between shear stress and shear rate at the wall ($\gamma = (\tau/\rho\nu)$), the onset shear rate at the onset of drag reduction can be determined from f^*, ($\gamma^* = (V^2 f^*/2\nu)$). Thus, the mean molecular weight of the PEO polymer solutions can be inferred from the P-K plots. Table 2.2 provides a summary of the non-degraded conditions tested, including mean molecular weight (M_w), the resulting slope increment (δ), onset wave number (W^*) and the shear rate at the onset of drag reduction (γ^*). These results demonstrate that the onset of drag reduction does vary with mean molecular weight since the molecular weights shown are consistent with the manufacturer specified values.

Table 2.2: Summary of non-degraded samples tested in the pressure drop apparatus as well as the resulting slope increment (δ), onset wave number (W^*) and the shear rate at the onset of drag reduction (γ^*).

$M_w \times 10^{-6}$ (g/mol)	C range (ppm)	δ -	W^* at C_{max} (m^{-1})	γ^* (s^{-1})
0.6	100	3.1	93600	8100
0.6	500	7.5	85200	6090
1	500	13.5	71900	3050
2	50	5.2	63700	2250
2	50-500	14.5	47700	1950
4	5	6.13	30900	900
5	5	7.5	27800	697

2.3.2 Degraded bulk flow characterization

It is well documented that when the wall shear rate is sufficiently large, mechanical degradation via chain scission is possible. This has been demonstrated in Elbing et al. (2011), Yu et al. (1979) and Hunston and Zakin (1980). While a universal scaling law for chain scission based on the molecular bond strength is available from Vanapalli et al. (2006), PEO has an established empirical relationship for the shear rate at the onset of degradation (γ_d) for a given mean molecular weight, $\gamma_d = 3.23 \times 10^{18} {M_w}^{-2.20}$, determined in Vanapalli et al. (2005) and later used in Winkel et al. (2009). If the shear rate exceeds γ_d, the polymer chains will break and the mean molecular weight will decrease. Within the polymeric regime on a P-K plot, this is realized as data deviating from the logarithmic curve at higher $Re\sqrt{f}$ and bending back towards the P-K law as shown in Moussa and Tiu (1994) and Elbing et al. (2009). This empirical relationship was used to design the current pressure drop apparatus and select the operation range such that no degradation occurred prior to the pressure drop measurement section. However, downstream of the measurement section was a needle valve that controlled the flowrate, which produced sufficiently high shear rates to rapidly degrade PEO via chain scission (i.e. breaking of the carbon-carbon and carbon-oxygen bonds that make up the polymer backbone). Thus, mechanically degraded samples were produced by passing a sample through the pressure drop apparatus with the needle valve in a predetermined position prior to passing them through a second time to characterize the degraded samples.

An example of a characterization of a degraded sample from the current study is provided in Figure 2.4. Here a sample with an initial molecular weight $M_{wi} = 2 \times 10^6$ g/mol was degraded to $M_{wf} = 0.6 \times 10^6$ g/mol. For comparison, results from a non-degraded $M_w = 2 \times 10^6$ g/mol sample are also provided along with the P-K law (Eq. 2.3) and the MDR asymptote (Eq. 2.4). The impact of mechanical degradation on the polymer behavior is apparent from the onset of drag reduction for the degraded

sample shifted to the right (i.e. to high Reynolds numbers and shear rates) compared to the non-degraded sample. This is consistent with Vanapalli et al. (2005) and Vanapalli et al. (2006), stating that the lower the mean molecular weight the higher the shear rate at the onset of drag reduction. A summary of the degraded results

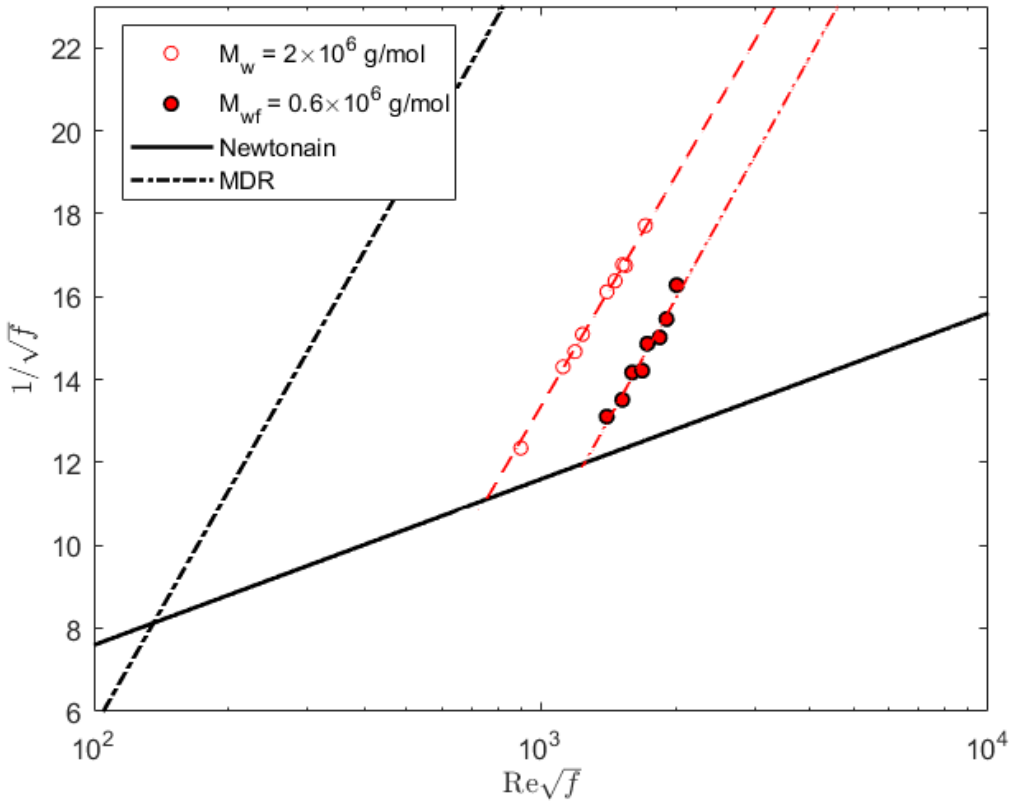

Figure 2.4: P-K plot using PEO at an initial $M_w = 2 \times 10^6 g/mol$ and c = 500 ppm. One of the samples was degraded to a lower molecular weight ($M_w = 0.6 \times 10^6 g/mol$) while the other was non-degraded

is provided in Table 2.3, which includes the initial molecular weight (M_{wi}) and final molecular weight (M_{wf}) as well as the polymeric regime characterization parameters. P-K plot data points for each test condition is given in tables 5.1 - 5.6 (see Appendix).

Table 2.3: Summary of degraded PEO samples tested in the pressure drop apparatus.

$M_{wi} \times 10^{-6}$ (g/mol)	$M_{wf} \times 10^{-6}$ (g/mol)	C (wppm)	$Re_D \times 10^{-3}$ at C_{max} range -	δ -	γ^* 1/s	$\gamma \times 10^{-3}$ 1/s
5	1.1	500	15 - 25	22.5	2800	4.2 - 8.1
4	1.3	500	15 - 30	20.6	3000	4.5 - 12
4	1.6	50 - 500	12 - 28	4.5 - 11.0	1600	1.8 - 10
5	2.1	500	12 - 24	16.6	2000	3.3 - 7.6
5	3.7	5	8 - 24	6.1	900	1.2 - 8.8
2	0.6	18 - 31	3.5 - 10.1	60-90	1200	7.7 - 15

2.4 Discussion and Analysis

2.4.1 Drag reduction performance

PDR generally is defined based on the reduction of the wall shear stress relative to the Newtonian (e.g. water) flow. Consequently, the common drag reduction (DR) definition is based on a comparison between the polymer modified wall shear stress (τ_p) and the Newtonian wall shear stress (τ_N), DR=$(\tau_N - \tau_p)/(\tau_N)$. As previously observed in the P-K plots, the drag reduction is dependent on the solution concentration, molecular weight and Reynolds number. While these drag reduction levels can be iteratively computed for every test condition, it is more efficient to quantify the drag reduction efficiency of the polymer solution via comparison of the change in the slope relative to the P-K law (i.e. the slope increment, δ). Thus to quantify the impact of mechanical degradation on the drag reduction ability of the polymer, degraded and non-degraded samples with the same onset of drag reduction (i.e. nominal mean molecular weight) and concentration were characterized and their resulting slope increments compared. The degradation procedure was tuned such that PEO samples with a nominal initial molecular weight between $1{\times}10^6$ and 5×10^6 g/mol were degraded to match the onset of drag reduction condition (i.e. mean molecular weight) as the non-degraded samples, which ranged from 0.6×10^6 to 4×10^6 g/mol.

Degraded samples are compared with non-degraded samples at the same onset of drag reduction condition (i.e. mean molecular weight) in Figure 2.5. First, the examination of the samples that had $M_{wi} = 4 \times 10^6$ g/mol that were degraded to

$M_{wf} = 2 \times 10^6$ g/mol with either C = 100 ppm or 500 ppm shows excellent agreement between the degraded and non-degraded samples. The maximum relative difference between degraded and non-degraded samples was 5%, which is within the uncertainty of these measurements. However, the deviation does appear to increase slightly with increasing concentration with the degraded sample consistently having the slightly larger slope, which suggests that the slope increment could have a potential weak concentration dependence. These results indicate that within this range of conditions tested, mechanical degradation has a negligible impact on the drag reduction performance as long as the mean molecular weight (i.e. onset of drag reduction) was matched between samples. Based on observations from Gampert and Wagner (1985), this is because, within the range of Reynolds numbers tested ($Re_d < 35{,}000$), the longer chains do not show any preferential extensions over other comparable but slightly shorter chains. This difference in size of chain is not significant enough to drastically change the flow characteristics of the solution and, therefore, no significant difference in bulk behavior was observed. However, Figure 2.5 also includes a C = 500 ppm sample that had $M_{wi} = 2 \times 10^6$ g/mol that was degraded to $M_{wf} = 0.6 \times 10^6$ g/mol compared with a non-degraded $M_w = 0.6 \times 10^6$ g/mol sample. These samples reveal a significant difference in slope increment between the mechanical degraded and non-degraded samples. Once again, the degraded sample produces a larger slope increment (i.e. more efficient at reducing the drag). Since the concentration was matched with one of the $M_{wi} = 4 \times 10^6$ g/mol conditions, these results indicate that there is a dependence on the initial and/or final molecular weights of the polymer solution in this regime of original, non-degraded (starting) molecular weights. This dependence on molecular weights indicates that the magnitude of drag reduction rather strongly depends on the largest molecular weight chains present in the solution. Gampert and Wagner (1985) showed that a Reynolds number of 35,000 was enough to degrade the fractions of large chains. Since the Reynolds number range of

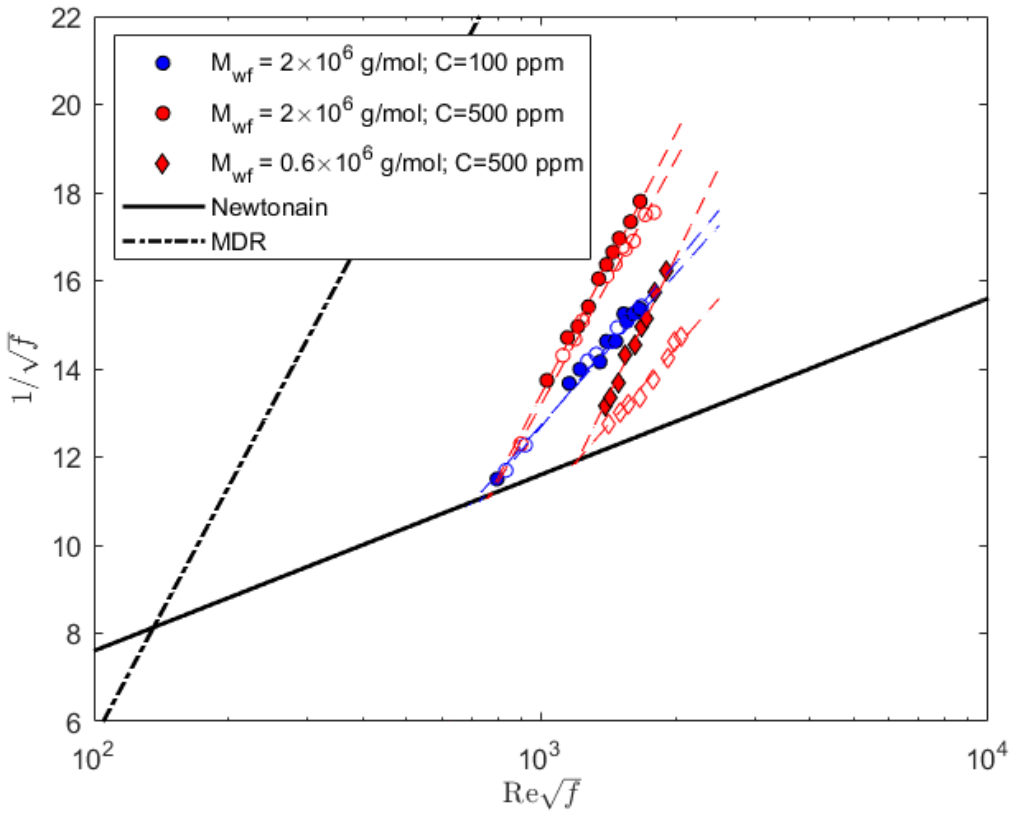

Figure 2.5: P-K plot comparing degraded and non-degraded samples with $M_{wf} = 2 \times 10^6$ g/mol or 0.6×10^6 g/mol. Filled markers represent degraded samples, open markers are non degraded at the same mean M_w

these experiments are above 20,000, the observations made with the mentioned molecular weight regimes points to the active participation of the long chains because they are stretched preferentially within the range of shear fields imposed by the Reynolds number. It is worth mentioning that in general these deviations were not strongly dependent on polymer concentration for a given molecular weight, which is convenient since the concentration range was dependent on the sample molecular weight given the flow setup (i.e. if concentration needed to be matched for all conditions, separate pressure drop apparatuses would have to be made for various molecular weight ranges).

Additional tests using non-degraded or initial molecular weights of 0.6, 1.0, 2.0, 4.0 and 5.0×10^6 g/mol showed similar trends. While slope increment is rela-

tively independent of the pipe diameter, it is sensitive to the polymer concentration, polymer-solvent combination and molecular weight as shown in Virk (1975). This prevents a simple comparison of variation in slope increment between degraded and non-degraded samples since the polymer concentration could not be matched for all combinations (i.e. higher molecular weight samples required lower concentrations than lower molecular weight samples). However, Virk (1975) compared numerous combinations of polymer types and solvents and showed that the slope increment is well approximated as being proportional to the square root of concentration. This relationship is shown in Figure 2.6 with all the best fits curves having slopes of 0.5. Note that a power-law fit to the raw data produces exponents that were within $\pm 5\%$ of 0.5 for all conditions. These results also show the sensitivity of the slope increment to molecular weight as well as the discrepancy observed in Figure 2.5 between the degraded and non-degraded $M_w = 0.6 \times 10^6$. If the molecular weight (i.e. onset of drag reduction) and the polymer-solvent (PEO-water) are matched, the degraded and non-degraded samples should produce the same δ versus C curves if the drag reduction performance has been unaltered. Thus a robust means of quantifying the deviation between the degraded and non-degraded samples is to examine the difference in the slope increment for a given concentration. Based on the previous observations, the deviation observed between the slope increment of degraded (δ_D) and non-degraded (δ_{ND}) samples appeared to be dependent on the initial and/or final molecular weight of the samples. Since the slope increment deviation should approach zero as degradation approaches zero, a reasonable parameter to scale the deviation is the difference between the initial and final molecular weights. This difference was normalized with initial molecular weight to make the scaling parameter, $\zeta = (M_{wi} - M_{wf}/M_{wi})$. Figure 2.7 shows the deviation of the slope increment (δ_D - δ_{ND}) as a function of ζ. The first observation from these results is that for all conditions tested the slope increment of the degraded samples was higher than the non-degraded samples at the same

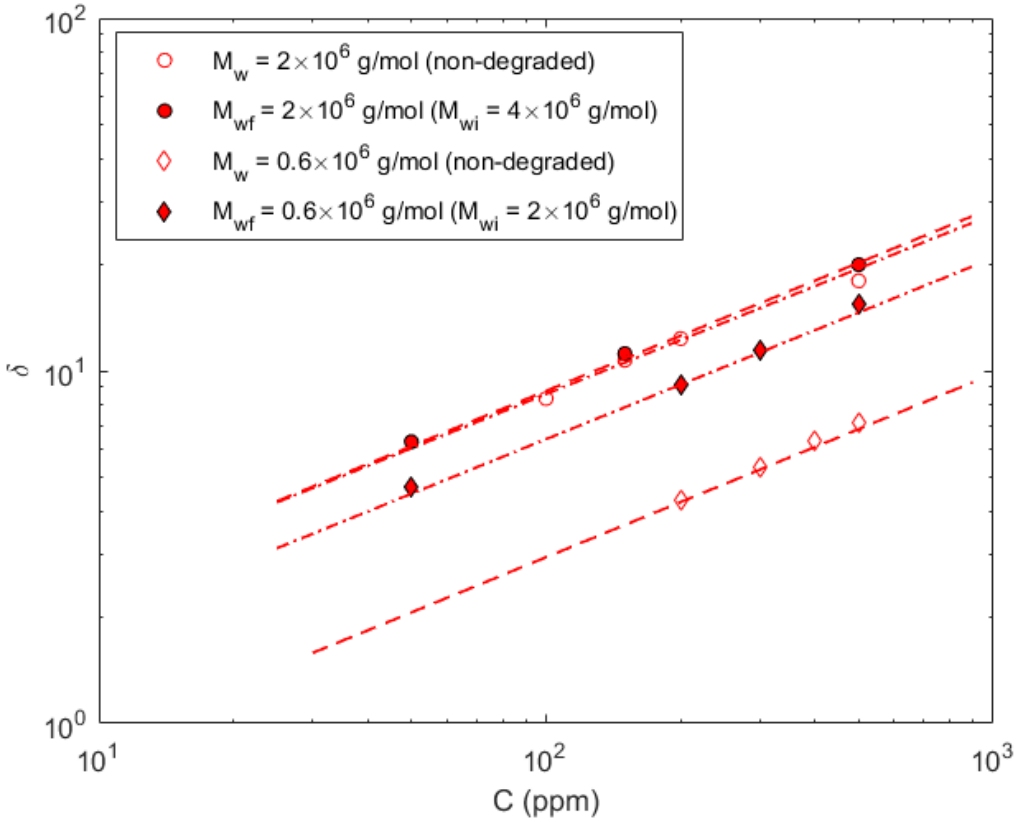

Figure 2.6: Slope increment versus concentration (C) for degraded and non-degraded samples of $M_w = 0.6 \times 10^6$ or 2.0×10^6 g/mol. The dashed lines are all best fit curves with a slope of 0.5

mean molecular weight. In addition, these results show a relatively small deviation for $\zeta < 0.6$, followed by a rapid increase in the deviation.

2.4.2 Polydispersity

Since testing, was performed within the same general flow operation range (i.e. $Re_d < 35000$, geometry, etc), the deviation must be the product of variations within polymer properties. Most PEO polymer properties (e.g. relaxation time, viscosity ratio, length ratio) are primarily a function of the molecular weight and concentration. Since the concentration and mean molecular weight (i.e. onset of drag reduction shear rate) are equal between the degraded and non-degraded PEO samples, the deviation in performance within the polymeric regime must be related to variations in

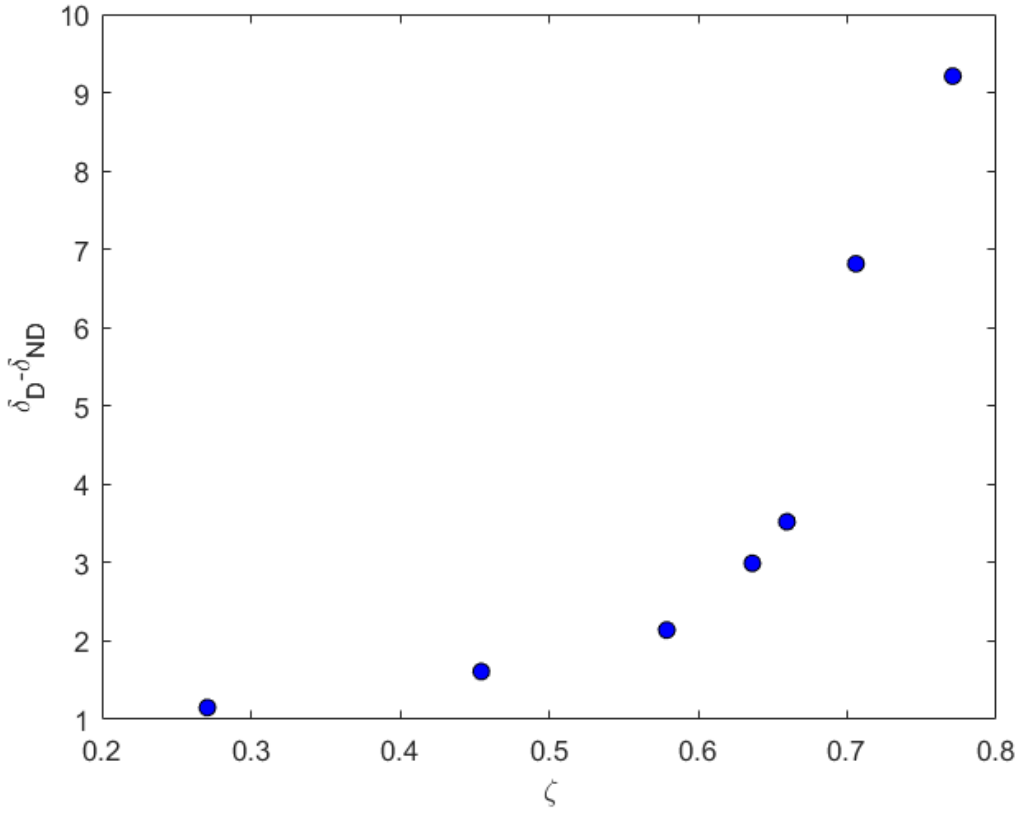

Figure 2.7: The difference between the degraded and non-degraded slope increments plotted versus the normalized difference between the initial and final molecular weights, $\zeta = (M_{wi} - M_{wf})/(M_{wi})$

the distribution of the molecular weight. This assessment is supported by Paterson and Abernathy (1970) that determined that the post-degradation molecular weight distribution (e.g. polydispersity) is critical to interpreting polymer flow properties. Furthermore, Hunston and Zakin (1980) studied the effect of mechanical degradation (flow-assisted degradation) on the molecular weight distribution of polystyrene. Turbulent measurements, like those in the current study, were used to broaden the range of conditions that could be studied with viscosity or GPC methods. This work showed that for polystyrene the onset of drag reduction was dependent on the molecular weight with the results biased towards the largest molecules in the sample, and that flow rate dependence was related to the shape of the top part of the molecular weight distribution. This supports the assessment that the deviations in slope in-

crement with the PEO samples were likely the product of a change in the molecular distribution (polydispersity) of the samples.

While this suggests that the deviations are related to changes in the molecular weight distribution, it does not explain the consistent improvement of the degraded samples relative to the non-degraded (at the same mean molecular weight) samples. The longer chain molecules have the greatest impact on determining the flow properties of a solution due to their preferential mode of extension as determined by Gampert and Wagner (1985) , which suggests that the current samples (especially those with the largest ζ) had a larger percentage of the longer chain molecules than the non-degraded samples. In general, mechanical degradation narrows the molecular weight distribution if the shear rate is relatively uniformly applied as shown in Yu et al. (1979) and Kim et al. (2000). Wall-bounded flows (e.g. pipes, boundary layers) do not have uniformly applied shear rates, which results in a relatively small percentage of the chains being stretched to lengths comparable to the polymer contour length (i.e. maximum polymer extension length) at any instance in time, as mentioned in Dubief et al. (2004) and Gupta et al. (2004). However, if the polymer chains are exposed to the turbulent wall-bounded flow for a sufficiently long period of time, a steady-state condition can be achieved once a sufficient number of stretching/degradation cycles are achieved, as discussed in Elbing et al. (2011). If the elongational rate far exceeds that of the critical elongational rate, then the midpoint scission assumption, discussed in Hinch (1977), Horn and Merrill (1984) and Odell et al. (1983), would be violated and the final (steady-state) distribution would be broader than the initial. This has computationally been shown in Sim et al. (2007). Prior to achieving steady-state conditions, the molecular weight distribution would be asymmetric and biased towards higher molecular weights because at each time step some percentage of chains would not have broken yet. This suggests that the current results correspond to an intermediate stage of degradation (i.e. prior to achieving steady-state behavior), which was

confirmed by comparing results from the water tunnel testing, whereby the polymer additives undergo infinitely many stretch-relaxation cycles to attain steady state M_w distribution.

The deviation in slope increment for $\zeta > 0.6$ is also indicative of the fact that a mere presence of a few long chain polymer molecules within a solution can be responsible for significantly increasing the drag reduction. That is to say, these small fractions of long chain molecules have a greater impact in defining the flow properties of a degraded sample, than the mean molecular weight of the sample as discussed in Paterson and Abernathy (1970). The validity of this claim within the specified regime of ζ, is also subject to the Reynolds number range tested, which for the current study was rarely above 30,000. For this range of Reynolds numbers, it could be justified to say that the long chain polymers show preferential extension over the shorter chains and therefore control flow properties of the solutions. Such a behavior is expected to be more pronounced when the disparity between short chains and long chains within a solution is large (disparity in terms of their molecular weight averages). Although Gampert and Wagner (1985) used artificially created polydispersed synthesized PAM solutions, they reached the same conclusions, which provides additional support to the validity of these conclusions.

The variational charactersitics for ζ dependence as shown in Figure 2.7, and more specifically the value where significant variation was observed, is most likely specific to the degradation process. If the residence time were increased, it is presumed that a larger value of ζ could be achieved without significant deviations in the slope increment since any variation would be the product of the broadening of the distribution, given the simulations of Sim et al. (2007), rather than an excess of larger molecules. As the ratio of the residence time to relaxation time becomes large, the steady-state molecular weight would be achieved and the impact of ζ is expected to significantly decrease if these assumptions are valid. This was tested by creating a

PEO polymer ocean with C = 100 ppm within the Oklahoma State University 6-inch low-turbulence, recirculating water tunnel. For more details on the tunnel design, the reader is referred to Elbing et al. (2018). This allowed the facility to be operated for as long as was required to achieve a steady-state mean molecular weight (based on the onset of drag reduction). In addition, the speeds were selected so that the steady-state molecular weights matched two of the non-degraded molecular weights (M_{wf} of 0.6×10^6 g/mol and 2×10^6 g/mol). The results for the steady-state degraded samples are shown in Figure 2.8 along with their corresponding non-degraded samples. The deviations in the slope increment for the 0.6×10^6 g/mol and 2×10^6g/mol samples were $\delta_D - \delta_{ND} < 0.5(\zeta = 0.8)$ and $\delta_D - \delta_{ND} = 1.3(\zeta = 0.5)$, respectively. These variations are within the measurement uncertainty and illustrate the difference from that observed in Figure 2.7, which supports the conjecture that these deviations can be mitigated if steady-state conditions can be achieved.

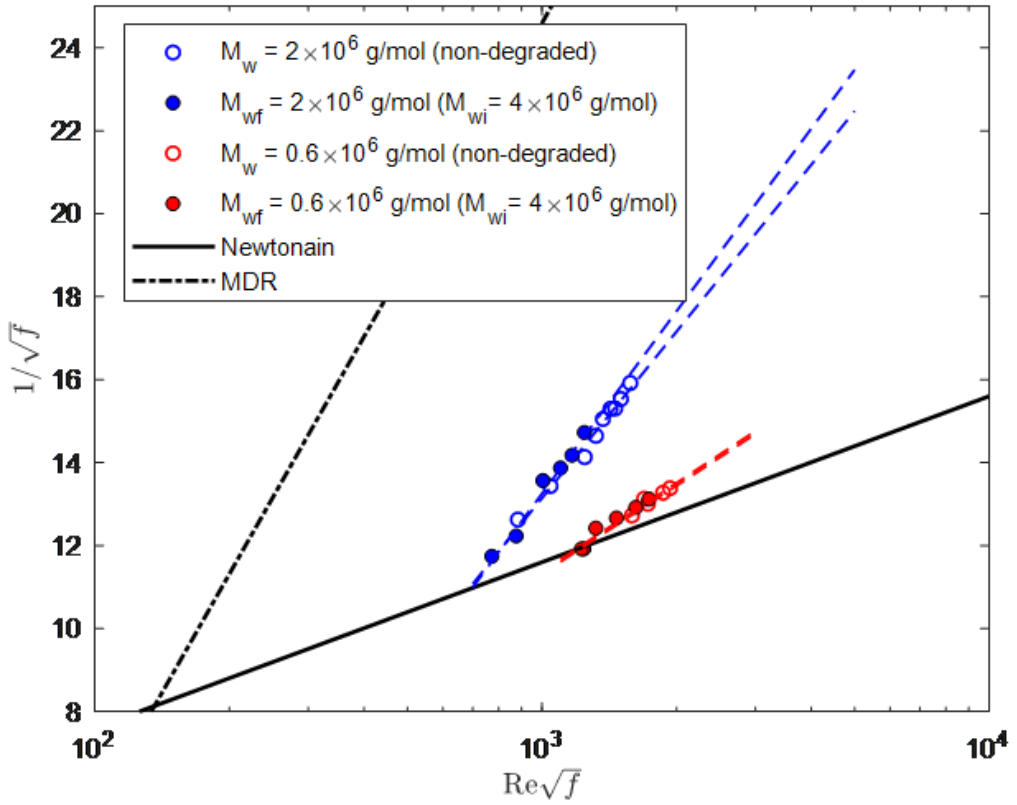

Figure 2.8: P-K plot comparing a steady-state degraded sample from a C = 100 ppm PEO polymer ocean in a recirculating water tunnel with that of a non-degraded sample.

CHAPTER III

Structure of Turbulence in Polymer Induced Drag Reduction

3.1 Background

3.1.1 Motivation

Mathematically, the Reynolds shear stress term in the RANS equation is indicative of the cross-gradient mixing process innate to turbulence, relaying that turbulence exhibits distinctive structural anatomy. Such cross gradient momentum diffusivity also hints on the possibility that the near-wall events are interlinked with those occurring farther away from the wall. Therefore, with such inter-dependency it is not a crude inference to make that spatio-temporal changes in one translates to modifications in the other. This approach can be particularly viable for the research on flow control applications via PDR which seeks a more fundamental answer to a basic question; what causes the drag and how the events responsible for drag are actually modified by polymer additives. There have been various attempts, which are discussed below in detail, to develop the context of forthcoming observations and their potential explanation. The view presented herein, primarily focuses on the topology of the near wall turbulent boundary layer flows and therefore, targets the physical aspect of the problem; mapping out the physics from the relevant mathematics. Initially, due to lack of computational capacities much of the work done has been purely empirical. Mathematics has been, and still continues to be, a major issue in the "unravelling of the problem" process due to its intractable nature. However, instead of directly delving in to the complex mathematics, one convenient way around the problem is to

retrieve the statistical details via experimental observations to extract a simple, yet meaningful, picture of the problem.

This investigation analyzes a developing turbulent boundary layer in a polymer ocean (uniform concentration) of polyethylene oxide (PEO). The polymer ocean minimizes the uncertainty in quantifying the polymer properties (e.g. Weissenberg number), which strongly depends on solution concentrations and average molecular weight. Determining the molecular weight for PEO can be done using the departure of the flow curve from the Prandtl-Karman law on the traditional P-K plot as discussed in chapetr II, but analyzing polymer drag reduction is significantly limited by the degradation of polymer molecule chains (i.e. polymer chain scission in turbulent flows). This shows that polydispersity, also subject to whether the molecular weights have achieved a steady-state distribution (Farsiani et al. 2019), effectively controls the flow characteristics. Thus, the effects of such intrinsic polymer properties have been considered to determine parameters, such as drag reduction, to parameterize the results. Such polymer dependent properties have been thought to have negligible effects previously. In essence, the current study aims to understand and provide a possible explanation of how polymer effects the coherency of induced motions and controls their spatial extent in the log layer and outer-wake regions as various regimes of DR are realized. Modifications to the basic structure of TBL are inferred from the changes in the structure inclination angles retrieved by the two-point normalized correlation plots, encompassing mostly the log layer. This has been compared with the literature to establish the legitimacy of this study, as well as further the aspect of modified TBL structure in PDR. Effects of polymer on auto-generation cycle of the hairpin structures are also observed and explained via literature to establish the consistency of this study and fortify the provided explanation.

The remainder of this chapter includes review of (3.1.2) Newtonian and (3.1.3) polymeric coherent structure literature followed by the (3.2) experimental methods,

(3.3) results, (3.4) discussion and (3.5) Coherent structure conclusions.

3.1.2 Literature review of Newtonian coherent structures

The relevance of a distinct near-wall turbulent flow structure makes the present study both natural and promising. Perhaps this has been the motivation for one of the earliest and groundbreaking works done by Kline et al. (1967) , revealing a pattern of distinctive, spanwise distributed, streaks of low momentum fluid in the viscous sublayer region. Kline et al. (1967) elaborated the concept proposed by Lighthill (1963), in which the wall normal velocity fluctuations were thought to be impressed on a spanwise vorticity element, dividing it into stretched and compressed segments. These segments then produce a spanwise variations of velocity, hence effecting the observed low speed streaks. A schematic of this process, as shown in Kline et al. (1967), for clarifying the physical picture involved in low-momentum streak formation is given in Figure 3.1.

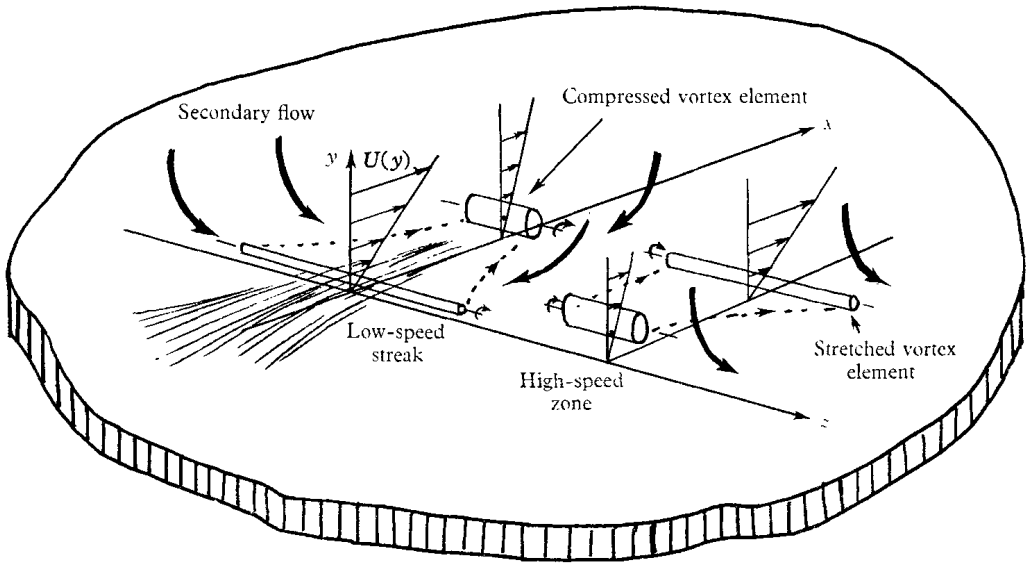

Figure 3.1: The mechanistic picture taken from Kline et al. (1967), detailing the proposition of Lighthill (1963) on low speed streak formation.

.

Soon thereafter, probe-based data and visual observations of Kim et al. (1971), Clark and Markland (1971), Grass (1971) and many others provided some of the first evidences of relatively long (often counter rotating pairs) quasi-streamwise vortices

and transverse vortices, complimented by a set of near-wall events, known as "sweeps" and "ejections", terminating in highly chaotic "bursting" events. This set forth the grounds for several vortex-based models to be proposed in the coming years following the legacy of Theodorsen (1952). Most notably, Hinze (1975) proposed that ejections, due to the lift-up of fluid between the vortex legs, give rise to an unstable shear layer, thereby producing the burst events. Although Blackwelder and Eckelmann (1979) found pairs of counter rotating streamwise vortices interacting with the outer region flow through a bursting mechanism as well, it was not until the work of Head and Bandyopadhyay (1981) that the most convincing visual evidence for these structures, which they termed as hairpin/horseshoe like vortices, came through with details of their orientation in turbulent boundary layers. Banking on the "physical insight" of Theodorsen (1952), Head and Bandyopadhyay (1981) made two important conclusions regarding the evolution of these vortices; (1) these structures get stretched and tend to be pushed towards the wall by the mean flow which intensifies the vorticity, causing self-induced velocities to raise these structures through the boundary layer until they reach about a 45° orientation (with respect to flow direction), at which point these opposing actions reach equilibrium, thereby maximizing turbulence production and (2) the outward growth of these structures is limited to the extent of the pre-existing strain field. The lifting up process as well as the unstable shear layer formation could be pictured as the spanwise vorticity effecting the low speed streaks as per Kline et al. (1967) and Lighthill (1963), lifting up as illustrated in Figure 3.2. Once the vortex lift-up initiates and it grows outwardly, the process is complimented by the sweep and ejection events that take place outboard and inboard of such a lifting vortex loop, as illustrated in Figure 3.3 (Robinson, 1991).

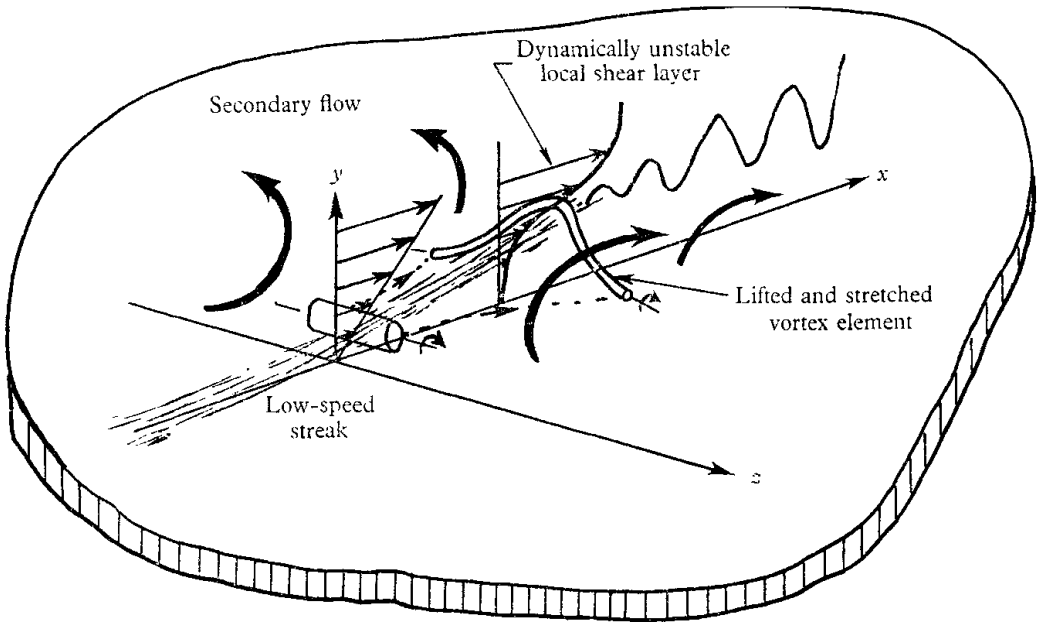

Figure 3.2: The Mechanistic picture taken from Kline et al. (1967), displaying vortex liftup and unstable shear layer formation.

Parallel computational efforts, like that of Blackwelder and Eckelmann (1979) served the needed mathematical guarantee for these laboratory observations. These developments meant that the coherent structure theory for near wall turbulence was not only physically sound, but also mathematically relevant. Such preceding developments and further visualizations of his own, inspired Smith (1984) to give a comprehensive model capturing the essential kinematics and dynamics of the near wall turbulent processes. A brief review of his model is in order for the sake of completeness and developing a relevant context to explain the forthcoming observations. The low speed streaks in the near wall region grows until a perturbation of sufficient strength impresses a local adverse pressure gradient, resulting in localized flow deceleration. The most likely victim of such decelerations are the low momentum fluid streaks because of their inherent inability to negotiate with the adverse pressure gradients. Inflectional profiles form at the low and high-speed fluid interface in the near wall region, setting them to oscillate under the background perturbations offered by the chaotic state of turbulent flows, thereby oscillating the low speed streaks. These

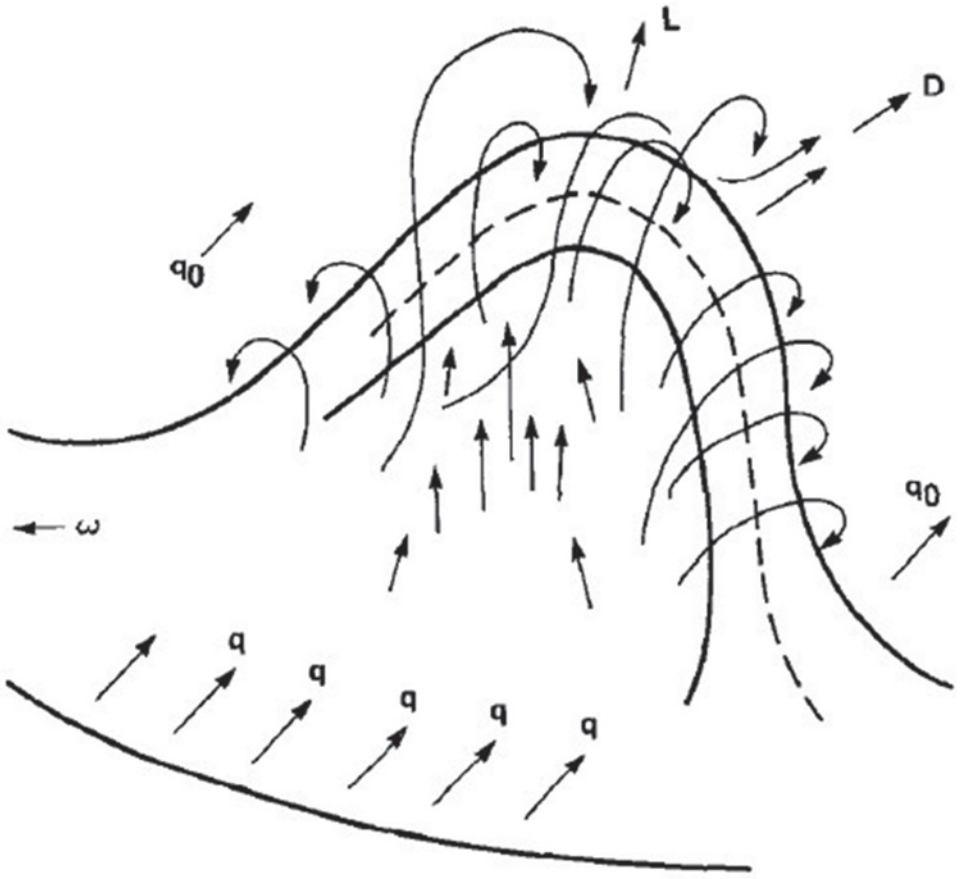

Figure 3.3: The origin of Q_2 and Q_4 events, as displayed in Robinson (1991), during vortex liftup

oscillations are then translated to perturbations in spanwise vortex sheet encompassing the streaks. This ultimately effects vortex concentrations rolling up and taking shape of the much-observed hairpin vortices. The growth of the hairpin, from here on, is governed by the antagonistic set of events; stretching of vortices by the mean shear flow and the self-induction effects of the hairpin structure. The stretching of the hairpin legs (appearing as counter rotating vortex pair in the near wall region) pumps the fluid away from the wall, whilst gathering more of the slow fluid between them as a consequence of vorticity intensification. This lifting up of the fluid constitutes the final stages of the burst event as described by Kim et al. (1971). More recent investigations, like that of Adrian et al. (2000) have shown that the protruding structures are crucial for the interactive mechanism taking place in the overlap region. This, as

an example for the Newtonian coherent structures is shown in Figure 3.4. 3.5 and 3.6 below. These figures tend to show that these structures convect at the local mean velocity while evolving in time and space simultaneously.

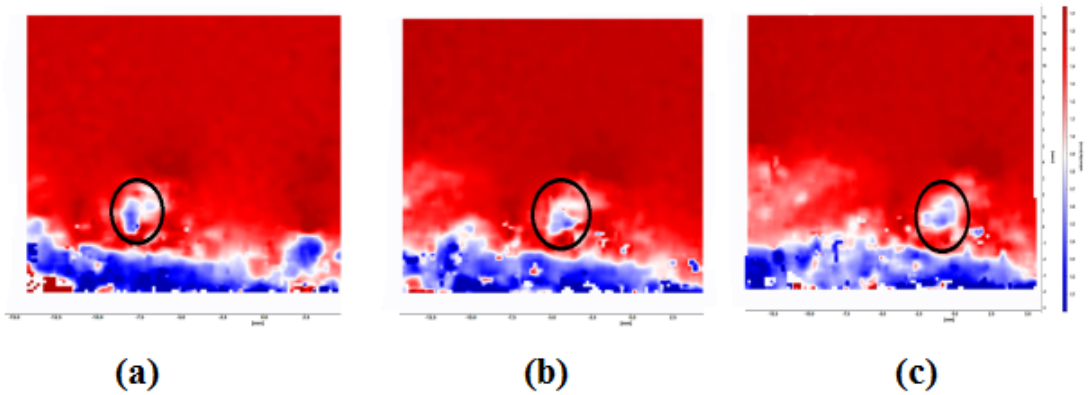

Figure 3.4: PIV snapshot of the large scale coherent structures highlighted (at (a) t= 1.0 ms, (b) t= 1.3 ms and (c) t= 1.6 ms

Complimenting the model proposed by Smith (1984) , a comprehensive statistical survey was then put forth by Robinson et al. (1989), which elaborated on the structural details of vortex distribution in terms of their circulation intensity-based strength, configuration, size and position within the turbulent boundary layer. The survey revealed that 70% of the vortices found in the near wall region, $y^+ < 100$, with the most intense of them residing within $y^+ < 75$, were streamwise oriented and 80% of the vortices surveyed in the region $80 < y^+ < 180$ were spanwise oriented. The survey also revealed that the spanwise oriented vortices were thicker in diameter as compared to the streamwise vortices; 74% of the spanwise vortices had their diameters between 30 and 70 viscous units and 73% of the streamwise vortices had their diameters between 10 and 40 viscous units. Based on circulation intensity strength,

streamwise vortices were far more intense than their spanwise counterparts.

3.1.3 Literature review of drag reduced coherent structures

Since the dominating momentum transfer in turbulence is due to Reynolds stresses, it should be well established by now that any drag reduction process must be associated with a change in the basic structure of the turbulent boundary layer; drag reduction calls for modifying the momentum exchange process between the outer and inner regions of turbulent boundary layers. Given their predominance in the near wall region and strong circulation intensity, streamwise vortices must be altered in geometry, orientation, position and circulation intensity to affect their contribution to the ejection, sweep and bursting processes. Initial investigations on polymeric flow boundary layer structure was done as early as Wells Jr and Spangler (1967) and Wu and Tulin (1972) to determine that polymer additives must be in the near wall region to produce drag reduction. Reischman and Tiederman (1975) further investigated to find that polymer additives had a pivotal effect on the mean velocity profiles in the buffer zone ($10 < y^+ < 100$). Later on, Tiederman et al. (1985) found that polymer additives had no effect on the linear sublayer region of the turbulent boundary layer indicating its passive role in reducing drag. Mounting evidence indicated that the buffer layer is central to the structure of turbulence and any reduction in drag must significantly alter its mechanics. On the parallel, flow visualization of drag reducing flows, as early as Donohue et al. (1972) and Achia and Thompson (1977), revealed that configuration of sublayer streaky structures significantly changed; the sub-layer low-momentum streak spanwise spacing increased with increasing drag reduction. Since the ejection and burst events follow in sequence, based on the model proposed by Smith (1984), any modified kinematics and dynamics of sublayer streaky structures must affect the ejection and burst events. Using "intensity of an event" by summing up the $u'v'$ over all three events (ejections, sweeps and bursts), Schmid (1984) found that, at low drag

reduction, such mean intensities differed significantly for the ejection type events as compared to Newtonian flows. Later on, Schmitt (1989) made the same observations with high drag reduction. This offered more support to the hypothesis that polymer additives inhibit the break-up of low speed streaks and therefore justifying the reduced frequency of the burst events as observed by Tiederman et al. (1985).

Gyr (2012) refers to a deficit in the Reynolds stress balance; shear and elongational processes alter the viscosity in the buffer zone. This is persistent with the ongoing theme that polymer additives interfere with the turbulent production/dissipation processes. There has been considerable evidence to suggests that the elastic stresses, termed as deficit in Reynolds stress balance, dampens the turbulent stresses. Gampert and Yong (1990) produced Joint Probablity Density Functions (JPDF) for the fluctuating wall normal and streamwise velocities, normalized by the near-wall units, to demonstrate that polymer additives significantly enhance anisotropy in the fluctuating motions. The damping of the wall normal velocity fluctuations is far more pronounced than the streamwise fluctuations, specifically in the buffer layer region of the boundary layer. Luchik and Tiederman (1988) further found out that lower threshold $u'v'$ events in the second and fourth quadrants are damped whereas the higher threshold $u'v'$ events are unaffected. Gampert and Yong (1990) used the time fractions for all the four quadrant events to characterize the effect of polymer additives on sweeps and ejections to find that these events are suppressed both in terms of their intensity and duration, specifically in the buffer layer region. The attenuated intensity of such events is a natural cause-and-effect type event following a decrease in vorticity and increase in size of the near-wall vortices, as predicted by the numerical computations of Gyr (2012).

Such a morphological introduction to polymer induced drag reduction has both fundamental and motivational reasons, therefore substantiating the need for the current study. Much less is known about how the polymer chains modify the structures

in the outer regions and their corresponding flow statistics, where significant velocity rise occurs at higher Reynolds numbers. A wide spectrum of structures in this region together with increasing Reynolds number, make flow simulations for these regions excessively expensive. Recent investigations such as that of Escudier et al. (2009), White et al. (2012) and Elbing et al. (2013) have also shown that the mean velocity profiles in the log-layer in the high drag reduction regime (HDR) i.e. DR $> 40\%$, show trends deviating from that of the low drag reduction regime (LDR), indicating polymer properties have more subtle role to play than flow properties. Therefore their characterization is a must for complete and meaningful analysis, thus requiring the study presented.

3.2 Experimental Overview

3.2.1 Test facility and model

The testing was performed in the Oklahoma State University 6-inch low turbulence recirculating water tunnel. The detailed structural design of the tunnel has been given in Elbing et al. (2018). It is worth mentioning that the overall design of the test section inlet allowed for a low inlet turbulence levels $< 0.3\%$ and negligible mean shear stress within the test section core. The flow measurements were acquired on the flat plate that formed the bottom wall of the water tunnel test section. The average surface roughness height was below 0.8 μm. This resulted in roughness height ($k^+ = k_c/l_v$) of less than 1.7. This allowed the surface to be assumed a hydraulically smooth surface. The coordinate system used throughout this study has the x origin at the test section inlet and extending in the downstream direction, the y coordinate increasing in the wall-normal direction with the origin at the test section center-line, and z extends in the spanwise direction completing a right-handed coordinate system.

3.2.2 Instrumentation

For data collection, time-resolved (particle image velocimetry (PIV) was employed. The velocity vectors were acquired at $x = 0.5$ m location in the mid-span plane of the test section. The laser setup comprised of high speed Nd:YLF laser (DM30-527, Photonics) spread into a thin sheet. The optical instruments included a high speed camera (M110, Phantom), recording at 2.0 kHz or 2.9 kHz and having a resolution of 1280 pixels $\times$ 800 pixels for a nominal field of view of 10 mm $\times$ 15 mm. The PIV timing, acquisition, and image processing were performed using a commercial software package (Davis 8.2.3, LaVision). For clarity, the illumination scheme has been shown in Figure 3.5.

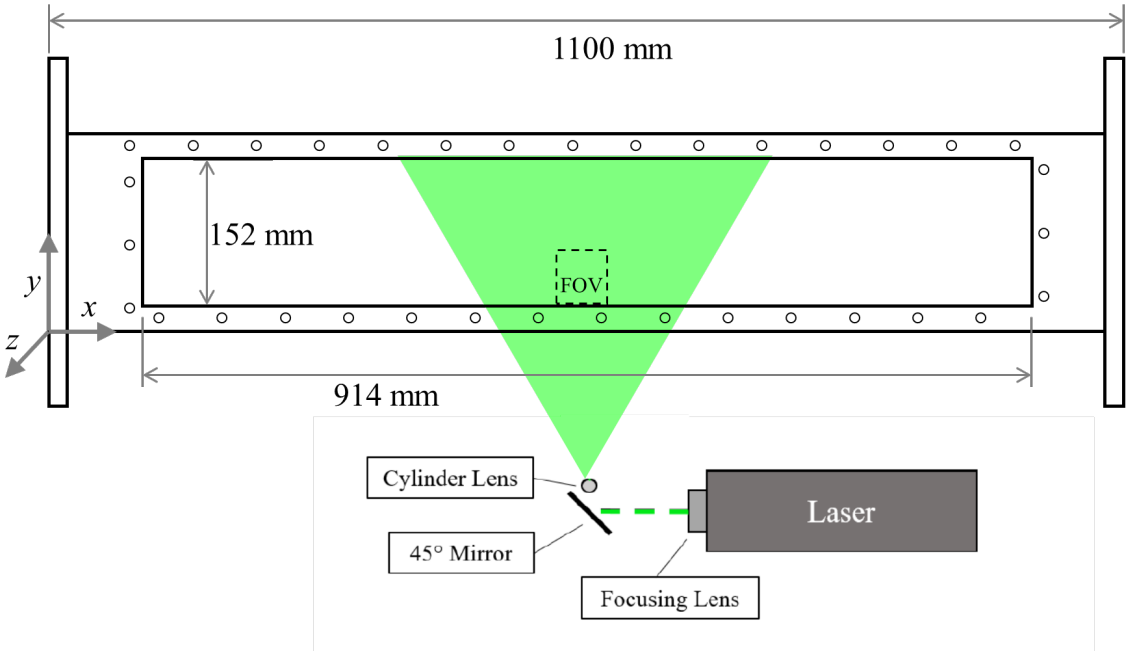

Figure 3.5: Schematic of the optical arrangement for the PIV measurements, including the nominal location of the field-of-view (FOV).

3.2.3 Polymer preparation and characterization

The preparation of polymer was done in a manner identical to that done for the study of degradation in the previous chapter. The polymer solutions had a constant concentration of 100 ppm. Thus all the solutions were considered dilute, given that

the overlap concentration was estimated to be $C^* \geq 517$ ppm. The only differing detail was that to enhance the scope of the study, the tests were also conducted with the 8 $\times 10^6$ g/mol (Sigma Aldrich model #: 732853) M_w grade of PEO. This helped realizing conditions near the MDR asymptote. The steady state molecular weight achieved during the course of the entire experimentation ranged from 0.7×10^6 g/mol to 4.2×10^6 g/mol. The determination of the intrinsic properties was done on the principals previously mentioned in the degradation chapter. To retrieve key flow parameters such as the drag reduction levels for a given polymer run, the same pressure apparatus used in Chapter II was used to determine the onset of drag reduction properties and intrinsic polymer properties, following the empirical drag reduction curve first proposed by Virk et al. (1967). This relation is given in Eq. (3.1),

$$\frac{\%DR}{C_m} = \frac{[C][\%DR]}{[C] + C_m}. \tag{3.1}$$

Here, [C] and [%DR] is the intrinsic concentrations and intrinsic drag reduction, respectively and pertain to a given polymer type and its M_w. A slight rearrangement of Eq. (3.1) gives a linear relation that can be used to analyze the drag reduction data efficiently. This form is given in Eq. (3.2),

$$\frac{C_m}{\%DR} = \frac{1}{[\%DR]} + \frac{C_m}{[C] + [\%DR]}. \tag{3.2}$$

While this empirical relation (Eq. 3.1) provides a relationship between the polymer concentration (C_m, and %DR for a given polymer solution), Eq. (3.2) can be used to plot the data and retrieve [C] and [%DR]. As has been mentioned above, the steady state molecular weight realized during the course of the experiments ranged from 0.7×10^6 g/mol to 4.2×10^6 g/mol. Once these conditions were realized by testing the samples taken directly from the tunnel for their M_w, fresh samples were then prepared and degraded to the corresponding molecular weights obtained. They

were then tested for their P-K plot slope increments. For each of the concentrations tested, f_p (implying Fanning friction factor for polymeric flow) was obtained using pressure drop apparatus data. The Re_d for each polymeric data point was then noted to retrieve the corresponding f_n (implying the Fanning friction factor for Newtonian flow) using Eq. (2.3) to estimate the average %DR for each concentration. For each M_w tested, the Eq. (3.2) was plotted to retrieve the [C] and [%DR] to determine the drag reduction values for the tunnel. However, following Choi and Jhon (1996), a correction factor of 1.25 must be applied to such intrinsic values to accurately the depict the wall shear stress for channel and flat plate flows. Using this scheme for the steady state M_w of 0.7×10^6 g/mol, 1.7×10^6 g/mol and 4.2×10^6 g/mol, the %DR values obtained were 25%, 58% and 78%, respectively. The data for this analysis is presented in Tables B.1 - B.9 (see Appendix). A summarized version of the intrinsic calculation is provided in Table 3.1 to effectively recap the flow conditions realized.

Table 3.1: Intrinsic concentrations and drag reduction values for the achieved steady state M_w. Note that %DR here reflects the %DR acheived in tunnel with 100ppm.

M_w (g/mol)	[C]	[DR]	$\%DR$
0.7×10^6	62.6	0.31	20
1.7×10^6	10.6	4.4	46
4.2×10^6	15.4	3.52	62

The conditions tested in the water tunnel covered a moderate range of momentum-thickness based Reynolds numbers, Re_θ. The minimum Reynolds number tested was of $Re_\theta = 800$ whereas the maximum Reynolds number realized was of 2900. Given the range of molecular weights tested, the Wiessenberg number varied from 0.22-3.26. This corresponded to the %DR levels of 25% to 78%, respectively. Other parameters such as the ratio of solvent viscosity to zero shear viscosity, μ^*, and the length ratio of the fully extended to coiled length of the polymer chain, (L), have been adjusted such that their variations have been kept minimal to prevent their effect on the obtained results.

3.2.4 Data analysis

The most relevant statistical quantity for the analysis of coherent structures is that of the fluctuating velocities. The usual decomposition of the mean and fluctuating velocity is adopted such that $\tilde{u}$ is the instantaneous velocity comprising of U, the ensemble average of $\tilde{u}$, and u, the fluctuating velocity. Therefore, the stream-wise correlation are based on the stream-wise fluctuating velocities and defined as in Eq. (3.3),

$$R_{uu}(x_{ref}, y_{ref}, \Delta x_{ref}, \Delta y_{ref}) = \frac{\overline{u(x_{ref}, y_{ref}) u(x_{ref} + \Delta x, y_{ref} + \Delta y)}}{\sigma_u(x_{ref}, y_{ref}) \sigma_u(x_{ref} + \Delta x, y_{ref} + \Delta y)}. \tag{3.3}$$

Here, x_{ref}, y_{ref} are the spatial location of the reference point, σ_u is the standard deviation of u at the specified location, the over-bar indicates an ensemble average, and Δx,Δy are the stream-wise and vertical separation distances from the reference location. The reason for selecting the correlations of the stream-wise velocity has been driven by the numerical simulations and empirical observations recorded in the literature; the anisotropy of the fluctuating flow field is more biased towards the stream-wise fluctuations while suppressing the fluctuations in the other two directions. Therefore, it is logical to observe the behavior of stream-wise correlations as they potentially have more information to reveal about the modified structure of the

near wall turbulence in polymeric flows. To increase the range of spatial separation, Taylor's frozen turbulence hypothesis was invoked. The approach of using velocity statistics to retrieve inclined motions has been used in a number of past studies. For instance Gampert and Yong (1990) have used JPDF to show that the elliptical shaped probability contours in the near wall region represent enhanced anisotropy for polymeric flows. Whereas, other attempts like that of Marusic et al. (2011) involve two-point correlations contour to estimate the orientational details of the dominant structures in the near wall region. Following Marusic et al. (2011), the two-point correlations of stream-wise velocity has been adopted with varying spatial separation such that for a given wall-normal position the stream-wise variance of the stream-wise velocity correlation is observed. In other words, Δy term in Eq. (3.3) has been kept zero to investigate how dominant is the anisotropic nature of the *flow scales* with varying levels of drag reduction .

3.3 Results

3.3.1 Mean velocity profiles

As a means of establishing a systematic approach to the current study, the mean velocity profiles of the Newtonian and non-Newtonian cases are shown first. In both cases, the canonical views established in the literature can be observed. In Figure 3.5, which includes the inner variable scaled mean velocity profiles for the Newtonian cases are the established law of the wall ($U^+ = (ln(y^+)/(\kappa) + B)$, which the current results are in close agreement with the law of the wall with $\kappa = 0.4$ and $B = 5.0$. For the three different Reynolds number, it can be observed that the profiles flatten out; indicating that such a velocity distribution persists through the entire boundary layer thickness.

The mean velocity profiles for the polymeric flows, as shown in Figure 3.6, include both the low drag reduction (LDR) and high drag reduction (HDR) regimes. For

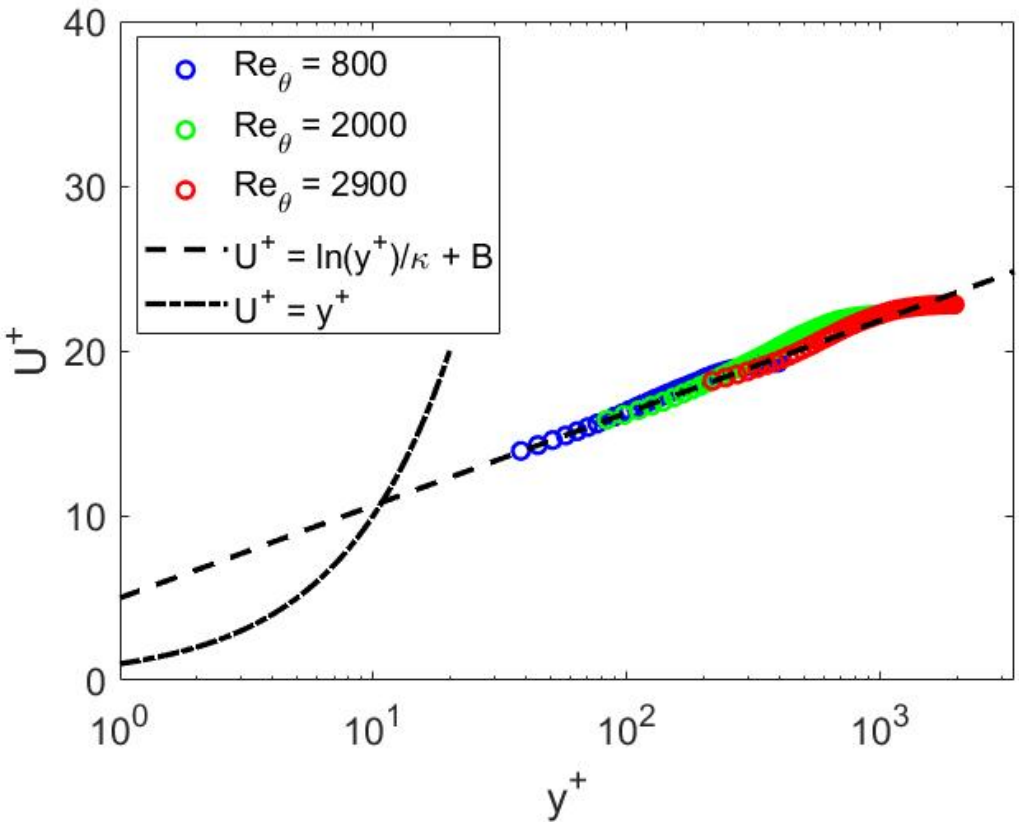

Figure 3.6: Inner variable scaled streamwise velocity profiles for water (Newtonian, DR = 0%). The profiles are compared with the viscous sublayer profile ($U^+ = y^+$) and the traditional log-law profile ($U^+ = (ln(y^+)/(\kappa) + B$) with $\kappa = 0.4$ and B = 5.0.

comparison the 0% DR case (Newtonian), the log law of the wall and the ultimate profile are included. For each of the conditions, the corresponding Wiessenberg number is also given so as to ascertain the growing influence of the polymer properties on the flow field. It can be observed that the canonical view of the Newtonian plug concept is seen to be verified by the mean velocity profiles when in the LDR regime; the main effect of the polymer additives in LDR is the parallel shift of the velocity profiles in the core region (i.e. changes in B). Whereas, for HDR regime (i.e. DR > 40%) the mean velocity profile appears to be challenging the classical view presented by Virk (1975); in addition to slope intercept (B) of the mean velocity profiles, the von-Karman constant (κ) is also a function of some polymer property, as first pointed out numerically and experimentally by White et al. (2012) and Elbing et al. (2013),

respectively. Furthermore, it can also be observed that with increasing DR levels, the logarithmic region is progressively compressed as the buffer layer becomes expanded, attesting to the long-held notion that such an increased elastic zone points for the visco-elastic nature of the flow at and near the MDR asymptote. These profiles also

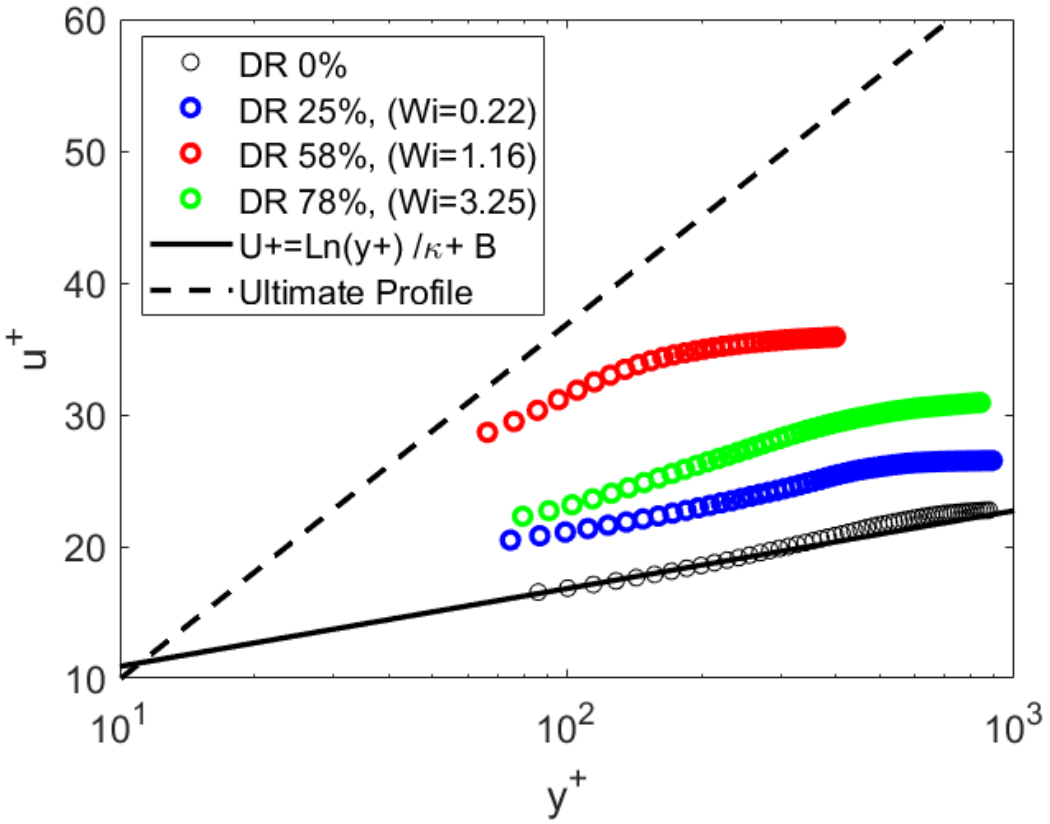

Figure 3.7: Inner variable scaled mean streamwise velocity profiles at three drag reduction levels (25%, 58% and 78%) with corresponding Weissenberg numbers listed. The polymer ocean concentration was fixed at 100 ppm and Re_θ=2000. The log-law, ultimate profile and water results (DR = 0%) are also included for comparison

serve to establish the baseline phenomenological structure of the turbulent boundary layer for both the Newtonian and non-Newtonian flows. Besides this, these profiles also help identifying the logarithmic region of the turbulent boundary layer for the subsequent two-point correlations and therefore makes it convenient to see how the flow structure within this region is modified by the the polymer additives.

3.3.2 Newtonian two-point correlations

Given that the focus of the current study is on the modifications within the overlap region (i.e. log-layer), the reference location for the two-point correlations shown in Figure 3.8 are selected to be well within the log region. This can be confirmed by using Figure 3.6 and observing that the $y^+{}_{ref}$ selected to between the bounds 148-250 indeed corresponds to the logarithmic region of TBL. Figure 3.8 is a two-point correlation plot in a purely stream-wise direction for Newtonian flows at $Re_\theta = 2000$. Note that the peaks at $\Delta x = 0$ are at unity because for these conditions it would be the normalized autocorrelations of the stream-wise fluctuating velocities.

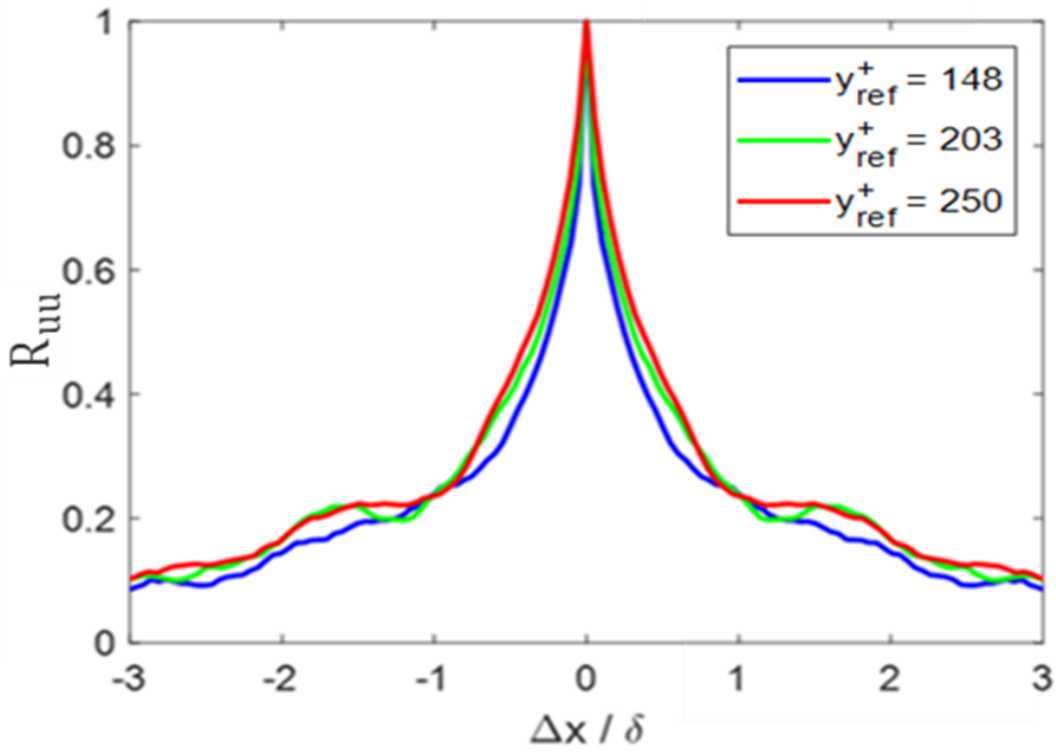

Figure 3.8: The two-point correlations of the streamwise fluctuating velocities in water (Newtonian) at $Re_\theta = 2000$ for varying reference heights with (b) $\Delta y^+ = 0$

3.3.3 Non-Newtonian two-point correlations

To present the polymeric counterpart of the two-point correlations presented above in Figure 3.8, Figure 3.9 shows the correlations of the streamwise fluctuating velocities

with purely streamwise separations (i.e. $\Delta y = 0$). Note that only one ${y^+}_{ref}$ was selected for each DR level in Figure 3.6 for clarity, and the selections were such that it depicts the events within the logarithmic region and its interactions with the outer-wake region. As has been pointed out previously, the peaks at $\Delta x = 0$ are at unity because for these conditions it would be the normalized autocorrelations of the stream-wise fluctuating velocities. Of particular note is the stream-wise scale captured in Figures 3.8 and 3.9; the scale has been significantly enhanced for the polymeric flow to observe the global effect of the polymer additives on the scales of motion in the logarithmic region. For a convenient comparison, Figure 3.9 also includes the 0% DR case (Newtonian flow) and in essence shows the transformations in the flow scales for conditions varying from no DR to near MDR asymptote (referring to 78% DR case).

There are various features worth noting in Figure 3.9. Such features of the plots for both the Newtonian and polymeric cases are explored in detail with reference to the most relevant literature and the mechanics of flow proposed in the following section. Note that the results presented herein form a particular case of a more comprehensive study done in Farsiani et al. (2019c).

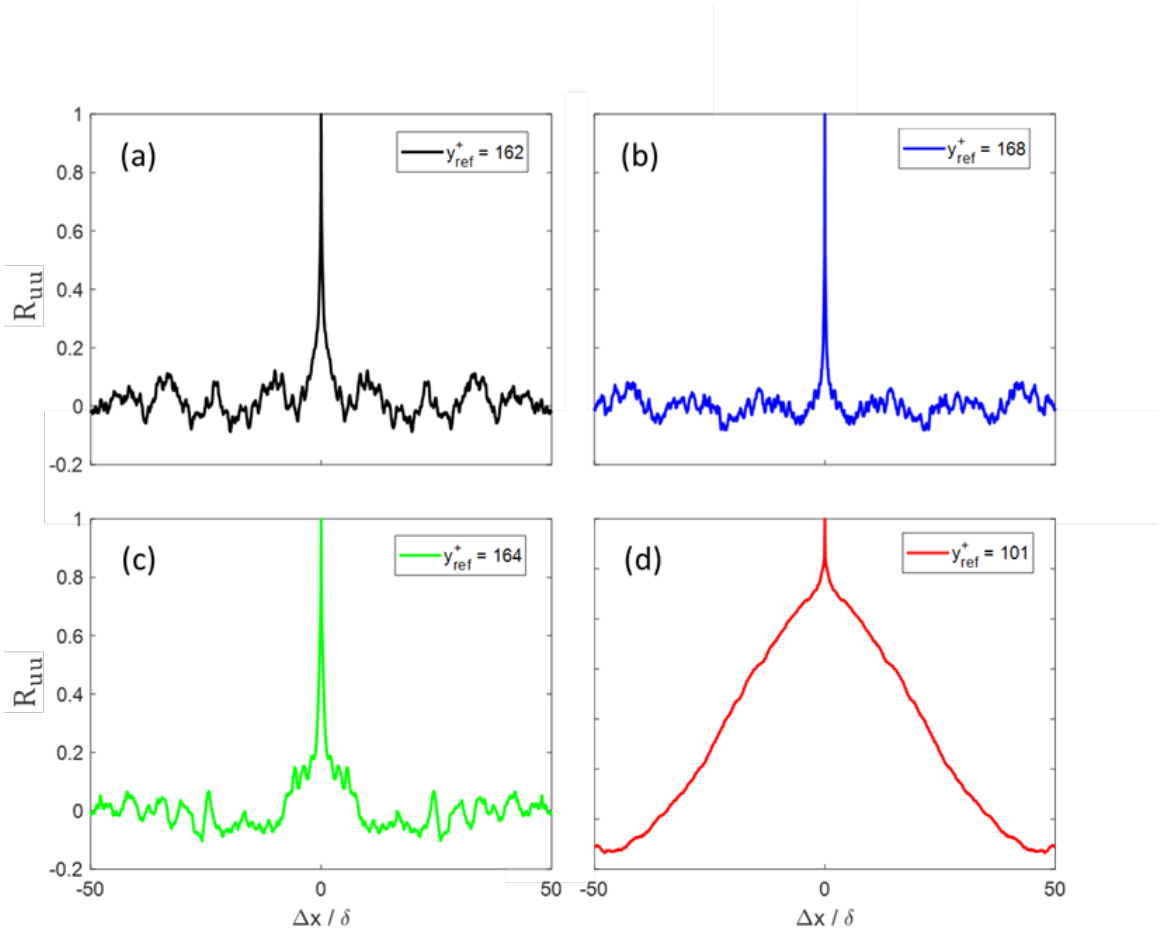

Figure 3.9: Two-point correlations of the stream-wise velocity fluctuations with $\Delta y^+ = 0$ and $101 \leq {y_{ref}}^+ \leq 168$ with (a) DR = 0%, (b) DR = 25%, (c) DR = 58% and (d) DR = 78%.

3.4 Discussion

3.4.1 Newtonian two-point correlations and the large scale motions

The general consensus on the morphology of coherent structures is that different manifestations of the same general structure (i.e. the hairpin/horseshoe vortex) is observed throughout the boundary layer, as discussed in Adrian et al. (2000). In particular, within the log-region of the TBL, the most commonly observed aspects of such structures are the "necks" of mature, older, hairpin vortices and the "heads" of developing, relatively younger, hairpins vortices as they protrude through the near-wall region of the TBL. The growth of these structures is therefore expected to be

influenced by the flow parameters. This was first put-forth by Head and Bandyopadhyay (1981), who saw that such structures thin out as Reynolds number is increased. As has been detailed in the section (3.1.2), the growth of such structures in the near wall region is influenced, in part, by the level of strain field imposed by the flow.

Flow visualization of hairpin vortices by Head and Bandyopadhyay (1981) and the more recent spectral coherence analysis of turbulent flow structures, presented by Deshpande et al. (2019), have also shown that they have an inclination of 45° relative to the downstream direction to maximize turbulence production and that this orientation is Reynolds number invariant, as concluded by Marusic and Heuer (2007). Given the orientation such structures adopt in the near wall region, it is logical to think that the flow statistics associated with coherent motion induced by such flow structures represent their spatial alignment. This is especially true considering the definition for coherent structures/motions put forward by Robinson (1991); *"a three-dimensional region of the flow over which at least one fundamental flow variable (velocity component, density, temperature, etc.) exhibits significant correlation with itself or with another variable over a range of space and/or time that is significantly larger than the smallest local scales of the flow*".

More detailed study on the evolution of such trademark turbulent flow structures was provided by Adrian et al. (2000). Adrian et al. (2000) concluded that the angle of inclination of the hairpins in the packets can vary depending on their location within the TBL. They are small close to the wall (quasi-streamwise vortices) and increases to around 90° for the head and the neck regions. Protruding heads adopt a near vertical orientation in the outer layer while in the near-wall region (referring to the core of log layer) they have the conventional 45° orientation in line with connecting neck regions of hairpin vortices. Therefore, the literature establishes that within the logarithmic region, coherent structures are on average expected to be oriented at a 45° position. It should be duly noted that such a taxonomy of structure represents a

baseline state of turbulent flow with Newtonian fluids, and since the problem of PDR is an enhanced state of turbulent flow, modified orientation and therefore dynamics of such coherent structures must be expected.

Another important aspect of such organized flow patterns was investigated by Adrian et al. (2000). Although the origin of such structures is tied to flow perturbations and instability mechanisms in the viscous sublayer and buffer Layer, as described in the section (3.1.2) on the literature review of Newtonian coherent strcutures, once fully developed -implying that their expanse is up till the outer region of TBL- these structures influence and control the flow patterns found therein. This resulted in the idea of Large Scale Motions (LSMs).It has been observed that these regions display LSMs, characterized by concatenation of the protruding hairpin structures, referred to as hairpin vortex packets. The back-flow motions (Q_2 events) induced by a single hairpin vortex is reinforced by the adjacent hairpins both in the downstream and upstream direction to form relatively long, uniform momentum zones. The mechanism for such uniformly retarded flow zones was suggested by Meinhart and Adrian (1995), and subsequently, observed from experiments by Adrian et al. (2000). The underlying idea for this concatenated formation is that individual hairpins serve to bolster the velocities induced by other similar hairpins within a packet to produce such strong flow patterns. A conceptual picture of such an interaction, as provided in Adrian et al. (2000) has been given for reference in Figure 3.10.

It can be seen in Figure 3.10 that vortex packets having similar kinematics and dynamics pair up to form vortex packets. However, such a concatenated formation may have certain prerequisites; the bolstering effect of the individual hairpins is only expected to occur when these hairpins are interacting with other hairpins that are similar in age, strength and convectional velocities. This is especially true given that the vortex annihilation process tends to consume weaker vortices and so prevents them from impacting the flow. Also that the age of an individual hairpin determines

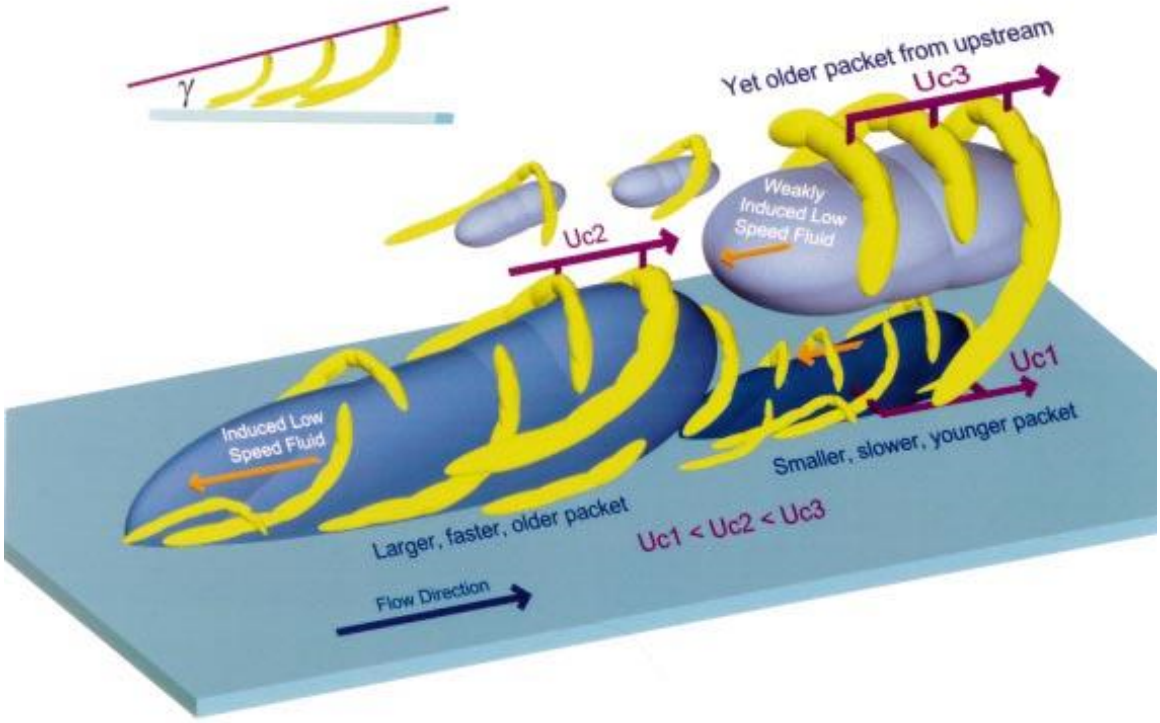

Figure 3.10: Conceptual picture given by Adrian et al. (2000) on the nested formation of hairpins to form hairpin packets and induce LSMs

the extent of its wall normal span in the TBL, the age factor is also an important criterion determining the spatial extent as well as the strength of such organized LSMs.

Given the picture presented above, the presence of LSMs suggest that regions of flow bearing such motions are basically regions of *uniform momentum*. The findings reported in Adrian et al. (2000) also suggest that the back-flow motions collectively induced by a number of hairpins in a hairpin vortex packet are essentially the zones of uniform momentum. This suggests that when the wall-normal separation for the two-point correlation estimates is set to zero ($\Delta y = 0$) then the curves should become symmetric for streamwise homogeneous flow. This indeed is observed in Figure 3.9 where $\Delta y = 0$ in Eq. (3.3) has been set to zero. The upstream versus downstream symmetry in Figure 3.9 strongly supports the concept of uniform momentum zones.

The dependence of R_{uu} (Δx,0) on the reference height appears to be consistent with a similar correlation plots computed by Monty et al. (2007). It is worth mentioning that the systematic dependence of R_{uu} (Δx,0) on the reference height appears to be relatively subdued for higher values of $y^+{}_{ref}$ i.e. $y^+{}_{ref} = 203$ and $y^+{}_{ref} = 250$. This shows increasingly uniform flow zones are achieved as outer regions of TBL are realized. This lends more support to the idea prevailed by Meinhart and Adrian (1995) and Adrian et al. (2000) and therefore forms as the stepping stone for the analysis of polymeric two-point correlations discussed next.

3.4.2 Polymeric two-point correlations and the modified flows

The crux of this study is to present ways in which the polymer molecules effect the flow statistics by presenting the two-point correlations of stream-wise velocities. As has been discussed at length above, the baseline structure of turbulent flow with Newtonian fluids is well established to be composed of uniform momentum zones. The Next logical question is to ask how do polymer additives modify/alter this baseline Newtonian flow structure? Figure 3.9 shows the correlations of the streamwise fluctuating velocities with purely streamwise separations (i.e. $\Delta y = 0$), which reveals additional details of how the polymers modify the flow statistics. Note that only one y_{ref} was selected for each DR level in Figure 3.9 for clarity, and the selections were such that it depicts the events within the log-layer and their interactions with the outer-wake region. Again, the deviations in the flow statistical trends are mild between water (DR = 0%; Figure 3.9a) and the LDR regime (Figure 3.9b), but as the DR level increases the differences become more apparent. Of particular note, the correlations persist longer spatially in the streamwise direction as DR increases. While the spatially averaged values of the normalized correlations increase with increasing DR, the fluctuations in the correlations are progressively reduced. This strongly suggests that the flow stabilization is spatially more prevalent with increasing DR. The

extent of such laminarization expands in the $x-y$ plane as a dominating effect of the polymer additives, which have been well-known to restructure the flow energetics.

Such plots for polymeric flow have several important inferences on how the polymers additives alter the structure of turbulent flows. Normalized correlations purely along the streamwise direction ($\Delta y = 0$) not only corroborate that the stretching of streamwise scales of the flow increases with increasing DR, but also that the polymer molecules interfere with the flow dynamics, thereby showing suppression in the fluctuations of the correlations. Since much of the high frequency content of the flow is essentially suppressed (referring to a comaparison between Figure 3.9a and Figure 3.9d) this indicates that polymer additives are actively engaged in suppressing the fluctuating content of the flow structures at higher frequencies. This serves as an experimental verification of the flow simulations from Kim and Sureshkumar (2013), featuring weakened vortices due to opposing torques by polymer body forces as described in Kim et al. (2007). Such vortices would then contribute less to the auto-generation process of hairpins, as Zhou et al. (1999) concludes.

Such attenuation of the fluctuating turbulent motions would suggest that the offspring shedding process of the primary hairpins (flow structures) has been curbed and that this restriction becomes stronger in HDR flows. However, modes of action on these structures by polymers is rather selective, based on the intrinsic polymer and flow properties. Swirling-strength based time scales of the vortices suggest that the shorter the time scale, the stronger the structure. This would increase the local Weissenberg numbers and therefore the probability of being attenuated by the stretching action of the polymers. Since the most intense of these vortices are in the buffer-layer, in the LDR the effect of polymers would remain within the buffer-layer. This explains the mild transition in observation between DR = 0% and DR = 25% for all correlations in the log-region. Mild transitions, however, do not suggest that there is "virtually" no effect of polymer additives on the log-layer.

It is clear that the "domino effect" of the weakened hairpin/quasi-streamwise vortices or QSVs is to make the log-region structures more inclined towards the flow direction. But as higher Weissenberg numbers are achieved, the polymers start effecting the less energetic vortex regions (heads and necks) found in the log layer directly. This could be attributed to the polymer relaxation times being significantly larger than the largest time scales associated with the vortex structures of the TBL. The reduced offspring shedding activity of the vortices, can potentially explain the enhanced correlations observed over long streamwise scales in Figure 3.9 . The fact that the structures are far apart, is compensated by their flattened orientation. Being targeted by the polymers based on their strengths, vortex structures with similar strength could weaken simultaneously, which aids in preserving the coherence of the eddying structure. The weakening of the structure by the polymer additives has several other important ramifications. The idea that polymer molecules offer counter torques, as introduced by Dubief et al. (2004) and Kim et al. (2007), would also mean that the vorticity intensification, otherwise induced by the mean shear flow, is now being opposed by the polymer molecules so that vortex structures are essentially *less potent* in making contributions to the Reynolds stresses via Q_2 and Q_4 events. This would suggest *laminarization* of the flow, as observed on comparing Figure 3.9a and Figure 3.9d.

To understand the abstract concept put forward in the current discussion, reconsider Figure 3.10. The preferential charge of the polymer molecules on the swirling strength of the vortex structures impact their potency to shed offsprings. This means that in a given packet of vortex structures at a given y^+ value, the number of hairpins will be lesser and less intense on average, based on their swirling strength. This, therefore, means that the fluctuations in the flow are more likely to be correlated over longer streamwise distances since the flow structure responsible for the fluctuations are far between as well weaker in comparison to their Newtonian counterpart. The

picture proposed herein compliments the general notion that polymer molecules are responsible for the enhanced anisotropy of the flow. This has been the conclusion of several studies done in the past including that of Warholic et al. (2001) and Gampert and Yong (1990), which focused on the inner region (i.e. viscous sublayer and buffer layer). It is worth mentioning that the works quoted above with regard to polymeric flows being more anisotropic than their Newtonian counterparts, talk in terms of anisotropy for the fluctuating flow fields. Whereas, the results shown here suggest that much like the fluctuating flow field in the viscous sublayer and buffer layer, it is the flow scales in the logarithmic region that tend to be significantly stretched in the streamwise direction therefore promoting anisotropy.

CHAPTER IV

Summary and Conclusions

4.1 Polymer degradation

The current study used a turbulent pipe flow experiment to do a comparative analysis between mechanically degraded polymer (PEO) solutions and non-degraded polymer (PEO) solutions at the same mean molecular weight. Degraded samples were produced via passing samples through a pipe that included a precisely positioned V-shaped needle valve. The degradation resulted in an increase in the shear rates at the onset of drag reduction, for which Vanapalli et al. (2005) provided an empirical relationship between the onset of drag reduction shear rate and the mean molecular weight for PEO. The samples were degraded such that they produced mean molecular weights (onset of drag reduction shear rates) that matched, within $\pm 10\%$ of available non-degraded molecular weights. Characterization of the non-degraded samples produced bulk flow behavior that is consistent with previous PEO studies in the literature, such as that done in Virk (1975), Gampert and Wagner (1985), Vanapalli et al. (2005) and Elbing et al. (2009). Comparative analysis of the mechanically degraded samples (samples with different initial, but known, mean molecular weights degraded to a known final mean molecular weight) with the non-degraded samples at the mean molecular weight of the final state of the degraded samples produced the following primary conclusions:

- While some conditions showed good agreement in the slope increment between degraded and non-degraded samples (Figure 2.5), there were conditions that had significant deviations in the slope increment (drag reduction performance)

between the degraded and non-degraded samples, with the non-degraded samples consistently larger (more efficient).

- The deviation in slope increment scaled well with the normalized difference between the initial and final molecular weights, $\zeta = (M_{wi} - M_{wf})/(M_{wi})$ with the deviation increasing rapidly when $\zeta > 0.6$. However, it is expected that the exact value of this acceleration is specific to the degradation method, including the ratio of the residence time to the relaxation time.

- The deviations in drag reduction performance for degraded and non-degraded samples at a given molecular weight were attributed to deviations in the molecular weight distribution, which was supported by other observations in Paterson and Abernathy (1970) and Hunston and Zakin (1980). Furthermore, this behavior is likely enhanced prior to achieving steady-state molecular weight, when there would be an excess of longer polymer chains as discussed in Gampert and Wagner (1985). It indeed was the case for the majority of conditions presented.

- The amount of deviation can be reduced if steady-state conditions can be achieved. However, if the elongational rate far exceeds the critical elongational rate then the final molecular weight distribution could be broader, as in Sim et al. (2007), which could still impact the drag reduction performance.

These results provide criteria that should be followed if comparisons in drag reduction performance will be made between mechanically (flow-assisted) degraded and non-degraded samples. These results are particularly valuable when using high molecular weight PEO samples at relatively low concentrations (i.e. common drag reduction operation conditions) since the common viscosity and GPC approaches are not well suited for these conditions, as detailed in Berman (1977) and Gampert and Wagner (1985). This also enables a robust means of establishing polymeric oceans that can be compared with previous non-degraded samples, which can greatly simplify

fundamental PDR studies of developing turbulent boundary layers by removing the concentration dependence.

4.2 Structure of turbulence

The study presented in this chapter used two-point correlations of the streamwise velocity to investigate the impact of polymer flow additives on the near wall turbulent flow structure. Flow measurements were taken over a flat plate using time-resolved PIV. Following the approach of Marusic (2001), the correlations have been modified to capture flow statistics in purely streamwise direction at a given ${y_{ref}}^+$. The ${y_{ref}}^+$ was chosen to depict the correlation of events in the logarithmic region for Newtonian flow and their modifications with drag reducing polymer additives. Analysis of the flows has produced the following primary conclusion.

- Much like the anisotropy of the fluctuating flow field in the viscous sublayer and the buffer layer, flow scales in the logarithmic region tend to experience significant bias in the flow direction. This is apparent from the large scale streamwise distances that the correlations take to get to zero. This can easily be observed when comparing Figure 3.9a with Figure 3.9d.

- The polymer additives are observed to preferentially target the high frequency structure content of the flow. The complete suppression of the fluctuations in streamwise correlations for the DR 78% case (depicting events near the MDR asymptote) points towards this wiping out of high frequency content, given that polymers primarily target the strength aspect of the vortical structure by providing counter torques to their rotation, corroborating the findings of Dubief et al. (2004) and Kim et al. (2007).

- The transition in flow statistics for the logarithmic region of TBL from 0% DR case (Newtonian flow) to $DR < 40\%$ is rather mild, at least until the demarcation region between the LDR and HDR regimes of PDR. The reason for such preferred action is due to the polymer relaxation times and the associated swirling strength of the vortices, which is inversely proportional to the time

scales associated with such structures. Since the most intense vortices reside beneath the logarithmic layer, as discussed in Robinson et al. (1989), the effect of transition is more likely to be observed first in the buffer layer and then in the logarithmic layer as the level of DR increases.

The nature of the conclusions made in this investigation are of a fundamental nature, being in line with the objective of the study. As has been mentioned in the introduction, numerical investigations in the outer region of the TBL are significantly limited by the computational obstacles presented by the wide spectrum of structures present and the high Reynolds numbers involved. This combined with the rheological models associated with polymeric flows makes pursuing such flow fields numerically an expensive task. An investigation such as above, can be helpful in providing a convenient way around this obstacle by providing initial insights to the problem so that if needed, appropriate computational schemes could be developed.

4.3 Future work

Polymer characterization is an important, and one of the fundamental aspects of PDR. Herein, the problem has been tackled experimentally purely from the mechanical view point. This warrants the need for an investigation that focuses on the rheological aspect of the problem. In particular, investigating the visco-elastic concerns of the problem can help us refine our understanding of the polymer chain scission dynamics and help us better predict the flow properties of dilute polymer solutions. Besides establishing the need on fundamental grounds, similar experimentation must be done with other available grades of long chain polymers like poly-isobutylene; poly-isobutylene is currently being used in the Alaska oil pipeline as a flow conditioners. This will help establishing the universality of such a behavioral difference between degraded and non-degraded samples, albeit a similar attempt has been made in the current study.

The study of turbulence, by interpreting its structural makeup based on the relevant statistical detail, promises a wealth of knowledge on the near wall turbulence. Although experimental investigations have been instrumental in laying out the road map to be adopted in this regard, one of the major issues is related to accurately capturing the dynamics of polymer chain so that a localized estimate of the polymer related parameters, such as the Wiessenberg numbers, can be made. This requires an in depth investigations into the buffer layer and statistically backed estimate of the coherent structures therein. A myriad of numerical data is available on such investigations. Time is high that they be corroborated by some experimental data to establish sound physical models relating the near-wall and outer region events. This has potential implications on shaping the research on numerical models and computational schemes, as well as on our ability to crack the code of turbulence.

References

Achia, B. and Thompson, D. (1977). Structure of the turbulent boundary in drag-reducing pipe flow. *Journal of Fluid Mechanics*, 81(3):439–464.

Adrian, R. J., Meinhart, C. D., and Tomkins, C. D. (2000). Vortex organization in the outer region of the turbulent boundary layer. *Journal of fluid Mechanics*, 422:1–54.

Bailey Jr., F. and Callard, R. (1959). Some properties of poly (ethylene oxide) 1 in aqueous solution. *Journal of applied polymer science*, 1(1):56–62.

Berman, N. S. (1977). Drag reduction of the highest molecular weight fractions of polyethylene oxide. *The Physics of Fluids*, 20(5):715–718.

Blackwelder, R. F. and Eckelmann, H. (1979). Streamwise vortices associated with the bursting phenomenon. *Journal of Fluid Mechanics*, 94(3):577–594.

Bortel, E. and Lamot, R. (1977). Examination of the breakdown of high molecular weight polyethylene oxides in the solid state. *Macromolecular Chemistry and Physics*, 178(9):2617–2628.

Burger, E., Chorn, L., and Perkins, T. (1980). Studies of drag reduction conducted over a broad range of pipeline conditions when flowing prudhoe bay crude oil. *Journal of Rheology*, 24(5):603–626.

Choi, H. J. and Jhon, M. S. (1996). Polymer-induced turbulent drag reduction. *Industrial & engineering chemistry research*, 35(9):2993–2998.

Culter, J. D., Zakin, J. L., and Patterson, G. K. (1975). Mechanical degradation of dilute solutions of high polymers in capillary tube flow. *Journal of Applied Polymer Science*, 19(12):3235–3240.

De Gennes, P.-G. and Gennes, P.-G. (1979). *Scaling concepts in polymer physics*. Cornell university press.

Deshpande, R., Monty, J. P., and Marusic, I. (2019). Streamwise inclination angle of large wall-attached structures in turbulent boundary layers. *Journal of Fluid Mechanics*, 877.

Donohue, G., Tiederman, W., and Reischman, M. (1972). Flow visualization of the near-wall region in a drag-reducing channel flow. *Journal of Fluid Mechanics*, 56(3):559–575.

Draad, A. A., Kuiken, G., and Nieuwstadt, F. (1998). Laminar–turbulent transition in pipe flow for newtonian and non-newtonian fluids. *Journal of Fluid Mechanics*, 377:267–312.

Dubief, Y., White, C. M., Terrapon, V. E., Shaqfeh, E. S., Moin, P., and Lele, S. K. (2004). On the coherent drag-reducing and turbulence-enhancing behaviour of polymers in wall flows. *Journal of Fluid Mechanics*, 514:271–280.

Elbing, B., Winkel, E., Solomon, M., and Ceccio, S. (2009). Degradation of homogeneous polymer solutions in high shear turbulent pipe flow. *Experiments in fluids*, 47(6):1033–1044.

Elbing, B. R., Daniel, L., Farsiani, Y., and Petrin, C. E. (2018). Design and validation of a recirculating, high-reynolds number water tunnel. *Journal of Fluids Engineering*, 140(8):081102.

Elbing, B. R., Dowling, D. R., Perlin, M., and Ceccio, S. L. (2010a). Diffusion of drag-reducing polymer solutions within a rough-walled turbulent boundary layer. *Physics of Fluids*, 22(4):045102.

Elbing, B. R., Perlin, M., Dowling, D. R., and Ceccio, S. L. (2013). Modification of the mean near-wall velocity profile of a high-reynolds number turbulent boundary layer with the injection of drag-reducing polymer solutions. *Physics of Fluids*, 25(8):085103.

Elbing, B. R., Solomon, M. J., Perlin, M., Dowling, D. R., and Ceccio, S. L. (2011). Flow-induced degradation of drag-reducing polymer solutions within a high-reynolds-number turbulent boundary layer. *Journal of Fluid Mechanics*, 670:337–364.

Elbing, B. R., Winkel, E. S., Ceccio, S. L., Perlin, M., and Dowling, D. R. (2010b). High-reynolds-number turbulent-boundary-layer wall-pressure fluctuations with dilute polymer solutions. *Physics of Fluids*, 22(8):085104.

Escudier, M., Rosa, S., and Poole, R. (2009). Asymmetry in transitional pipe flow of drag-reducing polymer solutions. *Journal of Non-Newtonian Fluid Mechanics*, 161(1-3):19–29.

Farsiani, Y., Saeed, Z., and Elbing, B. R. (2019a). Drag reduction performance of mechanically degraded dilute polyethylene oxide solutions. *arXiv preprint arXiv:1907.07614*.

Farsiani, Y., Saeed, Z., and Elbing, B. R. (2019b). Drag reduction performance of mechanically degraded dilute polyethylene oxide solutions. *arXiv preprint arXiv:1907.07614*.

Farsiani, Y., Saeed, Z., Jayaraman, B., and Elbing, B. R. (2019c). Modification of

turbulent boundary layer coherent structures with drag reducing polymer solution. *arXiv preprint arXiv:1909.09202*.

Fontaine, A. A., Petrie, H., and Brungart, T. A. (1992). Velocity profile statistics in a turbulent boundary layer with slot-injected polymer. *Journal of Fluid Mechanics*, 238:435–466.

Fore, R. S., Szwalek, J., and Sirviente, A. (2005). The effects of polymer solution preparation and injection on drag reduction. *Journal of fluids engineering*, 127(3):536–549.

Fruman, D. and Aflalo, S. (1989). Tip vortex cavitation inhibition by drag-reducing polymer solutions. *Journal of fluids engineering*, 111(2):211–216.

Gampert, B. and Wagner, P. (1985). The influence of molecular weight and molecular weight distribution on drag reduction and mechanical degradation in turbulent flow of highly dilute polymer solutions. In *The Influence of Polymer Additives on Velocity and Temperature Fields*, pages 71–85. Springer.

Gampert, B. and Yong, C. (1990). The influence of polymer additives on the coherent structure of turbulent channel flow. In *Structure of turbulence and drag reduction*, pages 223–232. Springer.

Grandbois, M., Beyer, M., Rief, M., Clausen-Schaumann, H., and Gaub, H. E. (1999). How strong is a covalent bond? *Science*, 283(5408):1727–1730.

Grass, A. J. (1971). Structural features of turbulent flow over smooth and rough boundaries. *Journal of fluid Mechanics*, 50(2):233–255.

Gupta, V., Sureshkumar, R., and Khomami, B. (2004). Polymer chain dynamics in newtonian and viscoelastic turbulent channel flows. *Physics of Fluids*, 16(5):1546–1566.

Gyr, A. (2012). *Structure of Turbulence and Drag Reduction: IUTAM Symposium Zurich, Switzerland July 25–28, 1989*. Springer Science & Business Media.

Habibpour, M. and Clark, P. E. (2017). Drag reduction behavior of hydrolyzed polyacrylamide/xanthan gum mixed polymer solutions. *Petroleum Science*, 14(2):412–423.

Head, M. and Bandyopadhyay, P. (1981). New aspects of turbulent boundary-layer structure. *Journal of Fluid Mechanics*, 107:297–338.

Hinch, E. (1977). Mechanical models of dilute polymer solutions in strong flows. *The Physics of Fluids*, 20(10):S22–S30.

Hinze, J. (1975). Turbulence mcgraw-hill. *New York*, 218:457.

Horn, A. and Merrill, E. (1984). Midpoint scission of macromolecules in dilute solution in turbulent flow. *Nature*, 312(5990):140.

Hou, Y., Somandepalli, V., and Mungal, M. (2008). Streamwise development of turbulent boundary-layer drag reduction with polymer injection. *Journal of Fluid Mechanics*, 597:31–66.

Hoyt, J. (1972). A freeman scholar lecture: The effect of additives on fluid friction. *Journal of Basic Engineering*, 94(2):258–285.

Hunston, D. and Zakin, J. (1980). Flow-assisted degradation in dilute polystyrene solutions. *Polymer Engineering & Science*, 20(7):517–523.

Jr FE, B. and Koleske, J. (1976). Poly (ethylene oxide).

Kalashnikov, V. (2002). Degradation accompanying turbulent drag reduction by polymer additives. *Journal of Non-Newtonian Fluid Mechanics*, 103(2-3):105–121.

Kim, C., Kim, J., Lee, K., Choi, H., and Jhon, M. (2000). Mechanical degradation of dilute polymer solutions under turbulent flow. *Polymer*, 41(21):7611–7615.

Kim, H., Kline, S., and Reynolds, W. (1971). The production of turbulence near a smooth wall in a turbulent boundary layer. *Journal of Fluid Mechanics*, 50(1):133–160.

Kim, K., Li, C.-F., Sureshkumar, R., Balachandar, S., and Adrian, R. J. (2007). Effects of polymer stresses on eddy structures in drag-reduced turbulent channel flow. *Journal of Fluid Mechanics*, 584:281–299.

Kim, K. and Sureshkumar, R. (2013). Spatiotemporal evolution of hairpin eddies, reynolds stress, and polymer torque in polymer drag-reduced turbulent channel flows. *Physical Review E*, 87(6):063002.

Kline, S. J., Reynolds, W. C., Schraub, F., and Runstadler, P. (1967). The structure of turbulent boundary layers. *Journal of Fluid Mechanics*, 30(4):741–773.

Kulik, V. (2001). Drag reduction change of polyethyleneoxide solutions in pipe flow. *Experiments in fluids*, 31(5):558–566.

Lander, M. (2018). *Preparation and Characterization of Polyethylene-Oxide (PEO) Solution*. PhD thesis.

Layec-Raphalen, M. and Layec, Y. (1985). Influence of molecular parameters on laminar non-newtonian and on turbulent flows of dilute polymer solutions. In *The Influence of Polymer Additives on Velocity and Temperature Fields*, pages 89–100. Springer.

Lighthill, M. (1963). Boundary layer theory.

Luchik, T. and Tiederman, W. (1988). Turbulent structure in low-concentration drag-reducing channel flows. *Journal of Fluid Mechanics*, 190:241–263.

Marusic, I. (2001). On the role of large-scale structures in wall turbulence. *Physics of Fluids*, 13(3):735–743.

Marusic, I. and Heuer, W. D. (2007). Reynolds number invariance of the structure inclination angle in wall turbulence. *Physical review letters*, 99(11):114504.

McGary Jr, C. (1960). Degradation of poly (ethylene oxide). *Journal of Polymer Science*, 46(147):51–57.

Meinhart, C. D. and Adrian, R. J. (1995). On the existence of uniform momentum zones in a turbulent boundary layer. *Physics of Fluids*, 7(4):694–696.

Monty, J., Stewart, J., Williams, R., and Chong, M. (2007). Large-scale features in turbulent pipe and channel flows. *Journal of Fluid Mechanics*, 589:147–156.

Moussa, T. and Tiu, C. (1994). Factors affecting polymer degradation in turbulent pipe flow. *Chemical Engineering Science*, 49(10):1681–1692.

Mysels, K. J. (1949). Flow of thickened fluids. US Patent 2,492,173.

Odell, J., Keller, A., and Miles, M. (1983). A method for studying flow-induced polymer degradation-verification of chain halving. *Polymer Communications*, 24(1):7–10.

Paterson, R. W. and Abernathy, F. (1970). Turbulent flow drag reduction and degradation with dilute polymer solutions. *Journal of Fluid Mechanics*, 43(4):689–710.

Perlin, M., Dowling, D. R., and Ceccio, S. L. (2016). Freeman scholar review: passive and active skin-friction drag reduction in turbulent boundary layers. *Journal of Fluids Engineering*, 138(9):091104.

Petrie, H., Deutsch, S., Brungart, T. A., and Fontaine, A. A. (2003). Polymer drag reduction with surface roughness in flat-plate turbulent boundary layer flow. *Experiments in Fluids*, 35(1):8–23.

Petrie, H., Fontaine, A., Moeny, M., and Deutsch, S. (2005). Experimental study of slot-injected polymer drag reduction. In *Proceedings of the 2nd International Symposium on Seawater Drag Reduction. Busan*, volume 605620.

Ptasinski, P., Nieuwstadt, F., Van Den Brule, B., and Hulsen, M. (2001). Experiments in turbulent pipe flow with polymer additives at maximum drag reduction. *Flow, Turbulence and Combustion*, 66(2):159–182.

Reischman, M. and Tiederman, W. (1975). Laser-doppler anemometer measurements in drag-reducing channel flows. *Journal of Fluid Mechanics*, 70(2):369–392.

Robinson, S., Kline, S. J., and Spalart, P. (1989). A review of quasi-coherent structures in a numerically simulated turbulent boundary layer.

Robinson, S. K. (1991). Coherent motions in the turbulent boundary layer. *Annual Review of Fluid Mechanics*, 23(1):601–639.

Schmid, A. (1984). Experimental investigation of the influence of drag reducing polymers on a turbulent channel flow. In *Third International Conference on Drag Reduction, Proceedings edited by RH Sellin, RT Moses, University of Bristol, paper B*, volume 12.

Sellin, R., Hoyt, J., Poliert, J., and Scrivener, O. (1982). The effect of drag reducing additives on fluid flows and their industrial applications part 2: Present applications and future proposals. *Journal of Hydraulic Research*, 20(3):235–292.

Shin, H. (1965). Reduction of drag in turbulence by dilute polymer solutions. Technical report, Massachusetts Inst of Tech Cambridge Dept of Chemical Engineering.

Sim, H., Khomami, B., and Sureshkumar, R. (2007). Flow–induced chain scission in dilute polymer solutions: Algorithm development and results for scission dynamics in elongational flow. *Journal of Rheology*, 51(6):1223–1251.

Smith, C. (1984). A synthesized model of the near-wall behavior in turbulent boundary layers. Technical report, Lehigh Univ Bethlehem PA Dept of Mechanical Engineering and Mechanics.

Somandepalli, V., Hou, Y., and Mungal, M. (2010). Concentration flux measurements in a polymer drag-reduced turbulent boundary layer. *Journal of Fluid Mechanics*, 644:281–319.

Theodorsen, T. (1952). Mechanisms of turbulence. In *Proceedings of the 2ˆ¡ nd¿ Midwestern Conference on Fluid Mechanics, 1952*.

Tiederman, W. G., Luchik, T. S., and Bogard, D. G. (1985). Wall-layer structure and drag reduction. *Journal of Fluid Mechanics*, 156:419–437.

Toms, B. (1949). Detection of a wall effect in laminar flow of solutions of a linear polymer. *Journal of Colloid Science*, 4(5):511–521.

Toms, B. A. (1948). Some observations on the flow of linear polymer solutions through straight tubes at large reynolds numbers. *Proc. of In. Cong. On Rheology, 1948*, 135.

Tropea, C. and Yarin, A. L. (2007). *Springer handbook of experimental fluid mechanics*. Springer Science & Business Media.

Vanapalli, S. A., Ceccio, S. L., and Solomon, M. J. (2006). Universal scaling for polymer chain scission in turbulence. *Proceedings of the National Academy of Sciences*, 103(45):16660–16665.

Vanapalli, S. A., Islam, M. T., and Solomon, M. J. (2005). Scission-induced bounds on maximum polymer drag reduction in turbulent flow. *Physics of Fluids*, 17(9):095108.

Virk, P., Mickley, H. S., and Smith, K. (1970). The ultimate asymptote and mean flow structure in toms' phenomenon. *Journal of Applied Mechanics*, 37(2):488–493.

Virk, P. S. (1975). Drag reduction fundamentals. *AIChE Journal*, 21(4):625–656.

Virk, P. S., Merrill, E., Mickley, H., Smith, K., and Mollo-Christensen, E. (1967). The toms phenomenon: turbulent pipe flow of dilute polymer solutions. *Journal of Fluid Mechanics*, 30(2):305–328.

Warholic, M., Heist, D., Katcher, M., and Hanratty, T. (2001). A study with particle-image velocimetry of the influence of drag-reducing polymers on the structure of turbulence. *Experiments in fluids*, 31(5):474–483.

Wells Jr, C. S. and Spangler, J. G. (1967). Injection of a drag-reducing fluid into turbulent pipe flow of a newtonian fluid. *The Physics of Fluids*, 10(9):1890–1894.

White, C., Dubief, Y., and Klewicki, J. (2012). Re-examining the logarithmic dependence of the mean velocity distribution in polymer drag reduced wall-bounded flow. *Physics of Fluids*, 24(2):021701.

White, C., Somandepalli, V., and Mungal, M. (2004). The turbulence structure of drag-reduced boundary layer flow. *Experiments in fluids*, 36(1):62–69.

White, C. M. and Mungal, M. G. (2008). Mechanics and prediction of turbulent drag reduction with polymer additives. *Annu. Rev. Fluid Mech.*, 40:235–256.

Winkel, E., Oweis, G., Vanapalli, S., Dowling, D., Perlin, M., Solomon, M., and Ceccio, S. (2009). High-reynolds-number turbulent boundary layer friction drag reduction from wall-injected polymer solutions. *Journal of Fluid Mechanics*, 621:259–288.

Wu, J. and Tulin, M. P. (1972). Drag reduction by ejecting additive solutions into pure-water boundary layer. *Journal of Basic Engineering*, 94(4):749–754.

Yarin, A. (1991). Strong flows of polymeric liquids part 2. mechanical degradation of macromolecules. *Journal of non-newtonian fluid mechanics*, 38(2-3):127–136.

Yu, J., Zakin, J., and Patterson, G. (1979). Mechanical degradation of high molecular weight polymers in dilute solution. *Journal of Applied Polymer Science*, 23(8):2493–2512.

Zaitoun, A., Makakou, P., Blin, N., Al-Maamari, R. S., Al-Hashmi, A.-A. R., Abdel-Goad, M., et al. (2012). Shear stability of eor polymers. *Spe Journal*, 17(02):335–339.

Zhou, J., Adrian, R. J., Balachandar, S., and Kendall, T. (1999). Mechanisms for generating coherent packets of hairpin vortices in channel flow. *Journal of fluid mechanics*, 387:353–396.

APPENDIX A

Polymer Characterization Data

Table A.1: P-K plot data points for polymer degradation pertaining to M_{wi} of 5×10^6 (g/mol) to M_{wf} of 1.1×10^6 (g/mol)

Re_d	f_p	$Re_d\sqrt{f}_p$	$(1/\sqrt{f}_p)$
17256	0.0044	1148	15.2
19540	0.0040	1233	15.8
22162	0.0035	1277	16.9
23461	0.0034	1333	17.3
25009	0.0033	1402	17.5

Table A.2: P-K plot data points for polymer degradation pertaining to M_{wi} of 5×10^6 (g/mol) to M_{wf} of 2.1×10^6 (g/mol)

Re_d	f_p	$Re_d\sqrt{f}_p$	$(1/\sqrt{f}_p)$
14558	0.0049	1008	14.3
15569	0.0048	1033	14.4
17252	0.0043	1109	15.2
19251	0.0040	1195	15.8

Table A.3: P-K plot data points for polymer degradation pertaining to M_{wi} of 5×10^6 (g/mol) to M_{wf} of 3.7×10^6 (g/mol)

Re_d	f_p	$Re_d\sqrt{f}_p$	$(1/\sqrt{f}_p)$
14558	0.0051	1082	14.0
18969	0.0043	1228	15.3
20152	0.0043	1308	15.2
22051	0.0042	1425	15.5
22951	0.0041	1462	15.7

Table A.4: P-K plot data points for polymer degradation pertaining to M_{wi} of 4×10^6 (g/mol) to M_{wf} of 1.3×10^6 (g/mol)

Re_d	f_p	$Re_d\sqrt{f}_p$	$(1/\sqrt{f}_p)$
19021	0.0048	1311	14.4
21040	0.0044	1369	15.1
23150	0.0039	1440	16.0
24502	0.0039	1522	16.1
26023	0.0037	1586	16.4

Table A.5: P-K plot data points for polymer degradation pertaining to M_{wi} of 4×10^6 (g/mol) to M_{wf} of 1.6×10^6 (g/mol)

Re_d	f_p	$Re_d\sqrt{f}_p$	$(1/\sqrt{f}_p)$
14900	0.0056	1115	13.3
15702	0.0056	1175	13.5
18670	0.0053	1359	13.7
18409	0.0053	1340	13.8
20120	0.0049		14.2

Table A.6: P-K plot data points for polymer degradation pertaining to M_{wi} of 2×10^6 (g/mol) to M_{wf} of 0.6×10^6 (g/mol)

Re_d	f_p	$Re_d\sqrt{f}_p$	$(1/\sqrt{f}_p)$
14917	0.0068	1208	12.1
17023	0.0062	1374	12.7
19980	0.0059	1502	13.0
20145	0.0059	1565	13.0
22145	0.0056	1638	13.4

Table A.7: P-K plot data points for non degraded polymer pertaining to M_w of 1.0×10^6 (g/mol)

Re_d	f_p	$Re_d\sqrt{f}_p$	$(1/\sqrt{f}_p)$
17210	0.0052	1249	13.9
18995	0.0049	1324	14.2
120454	0.0047	1441	14.6
22168	0.0045	1379	15.0
23257	0.0044	1500	15.0
24032	0.0042	1563	15.4

APPENDIX B

Intrinsic Drag Reduction Data

Table B.1: Data corresponding to intrinsic calculations for M_w of 0.7×10^6 g/mol, at concentration of 200ppm for an average %DR of 14.8

Re_d	f_n	f_p	$\%DR$
19246	0.0065	0.0059	9.5
21417	0.0063	0.0056	10.9
23602	0.0062	0.0052	15.5
24461	0.0061	0.0050	17.5
27419	0.0060	0.0048	20.6

Table B.2: Data corresponding to intrinsic calculations for M_w of 0.7×10^6 g/mol, at concentration of 300ppm fo an average %DR of 15.6

Re_d	f_n	f_p	$\%DR$
14044	0.0070	0.0067	11.7
18673	0.0065	0.0057	12.4
22146	0.0063	0.0053	15.0
24646	0.0061	0.0050	18.0
25761	0.0060	0.0048	21.4

Table B.3: Data corresponding to intrinsic calculations for M_w of 0.7×10^6 g/mol, at concentration of 400ppm for an average %DR of 16.7.

Re_d	f_n	f_p	$\%DR$
12400	0.0073	0.0065	11.4
17449	0.0066	0.0058	12.5
18921	0.0065	0.0057	15.2
21201	0.0064	0.0053	16.5
24567	0.0062	0.0050	18.5

Table B.4: Data corresponding to intrinsic calculations for M_w of 1.7×10^6 g/mol, at concentration of 8ppm for an average %DR of 20.6

Re_d	f_n	f_p	$\%DR$
14916	0.0069	0.0056	18.8
15727	0.0069	0.0056	18.8
18067	0.0066	0.0053	19.6
18459	0.0066	0.0052	21.2
19110	0.0065	0.0049	24.6

Table B.5: Data corresponding to intrinsic calculations for M_w of 1.7×10^6 g/mol, at concentration of 20ppm for an average %DR of 30

Re_d	f_n	f_p	$\%DR$
16210	0.0068	0.0050	26.4
18017	0.0066	0.0048	27.2
19201	0.0065	0.0043	33.8
19961	0.0064	0.0044	31.3

Table B.6: Data corresponding to intrinsic calculations for M_w of 1.7×10^6 g/mol, at concentration of 30ppm for an average %DR of 36

Re_d	f_n	f_p	$\%DR$
14329	0.0070	0.0050	28.5
17271	0.0067	0.0043	35.8
18324	0.0066	0.0042	36.3
20267	0.0065	0.0039	39.5

Table B.7: Data corresponding to intrinsic calculations for M_w of 4.2×10^6 g/mol, at concentration of 25ppm for an average %DR of 33.1

Re_d	f_n	f_p	$\%DR$
12426	0.0073	0.0053	27.4
15023	0.0070	0.0046	33.9
15966	0.0069	0.0043	36
18293	0.0067	0.0043	32.3

Table B.8: Data corresponding to intrinsic calculations for M_w of 4.2×10^6 g/mol, at concentration of 10ppm for an average %DR of 22.6

Re_d	f_n	f_p	$\%DR$
15449	0.0069	0.0054	21.8
16339	0.0068	0.0054	20.7
17006	0.0067	0.005	25.8
18416	0.0066	0.0049	25.8

Table B.9: Data corresponding to intrinsic calculations for M_w of 4.2×10^6 g/mol, at concentration of 5ppm for an average %DR of 12.6

Re_d	f_n	f_p	$\%DR$
9643	0.008	0.0070	11.5
13927	0.0071	0.0063	11.1
15979	0.0068	0.0059	13.8
116239	0.0068	0.0060	12.0

VITA

ZEESHAN SAEED

Candidate for the Degree of

Master of Science

Thesis: Characterization of Degraded Drag-Reducing Polymer Solution and its Impact on the Structure of Turbulence

Major Field: Mechanical Engineering

Biographical:

Education:

Completed the requirements for the Master of Science in Mechanical Engineering at Oklahoma State University, Stillwater, Oklahoma in December, 2019.

Completed the requirements for the Bachelor of Science in Mechanical Engineering at Ghulam Ishaq Khan Institute of Engineering Sciences and Technology, Topi, Pakistan, 2015.

Experience:

Worked as a Graduate Trainee at Fatima Fertlizers Ltd, Lahore, Pakistan.
Worked as an Entry Level Inspection Engineer at Fatima Fertlizers Ltd, Lahore, Pakistan.
Worked as an intern at American Energy Service (AES) Power Plant, Lalpir, Pakistan.

Student Affiliations:

APS